# EVALUATION OF BONE FIXATION IMPLANTS

A Thesis

by

LUKE ALLYN PERKINS

Submitted to the Office of Graduate Studies of
Texas A&M University
in partial fulfillment of the requirements for the degree of

MASTER OF SCIENCE

Approved by:

| | |
|---|---|
| Chair of Committee, | Hong Liang |
| Committee Members, | Ted Hartwig |
| | Mike McShane |
| Head of Department, | Jerald Caton |

December 2012

Major Subject: Mechanical Engineering

**ABSTRACT**

This research investigates the effects of the human body on the mechanical, chemical, and morphological properties of the surface of internal fixation devices. Stainless steel and titanium devices that had failed were provided from the Shandong Provincial Hospital in China, along with controls: implants that had never been used. Comparative study was conducted by evaluating properties of these implants before and after implanting.

The first part of the research was simulation, and a model of the human femur was analyzed in Solidworks. The stress analysis software simulated the stress distribution, the strain distribution, and the deformation pattern. Two cases were simulated: walking and car accident. The simulations showed the points of highest stress and led to the analysis of the implants that were used in those regions.

The next part of the research was to experimentally examine the properties and behavior of materials. Test samples fell into one of three categories: stainless steel femur implant, stainless steel tibia implant, and titanium femur implant. Material properties were characterized and effects of the human body on each of these groups were studied. Hardness was measured using Vickers hardness indentation. Surface roughness was analyzed using light interferometric technique. Potentiodynamic polarization analysis was performed to evaluate corrosive behavior before and after implanting. Scratch tests were conducted to evaluate wear resistance and the microstructure was analyzed to further understand the morphological changes that occurred of implanted samples.

Results showed that the human body generally degraded the material properties of the stainless steel femur implant.  There were no measurable effects of the same on stainless steel tibia and on titanium alloy.

**ACKNOWLEDGEMENTS**

I would like to thank my advisor, Dr. Hong Liang and my committee members, Dr. Hartwig and Dr. McShane for their advice, time, and wisdom.

I would like to thank all of the members in the Surface Science group at Texas A&M University for their patience and guidance throughout my experiments and research. There are many others I would like to acknowledge:

- Yan Zhou for your suggestions to my work and your faithful support through every step of my project.

- Sukbae Joo for your knowledge of various experimental procedures and for sharing with me first your hope in Christ.

- Michael Chiu for all of your helpful advice in formatting and writing my book (thesis).

- Xinliang He for your explanations of various experimental procedures.

- Dr. Cris Schwartz for the use of your lab and interferometry machine.

- Matthew Darden for the access to the Zygo machine and the explanation of how to use it.

- Jim Sajewski for all of the polishing equipment you let me use, and your insight into techniques for finishing odd job experiments.

- Shreyas Balachandran for your help in hardness testing and chemical etching.

Again I give a special thanks to Dr. Liang, who was the only professor who believed in me to finish my thesis within my personal deadline. The lessons I have

iv

learned from you go far beyond engineering. I have gone to Dr. Liang for personal advice, conversations about dogs, watching movies at her house with her nephew, and of course every pestering question I could come up with about my thesis (you shouldn't have given me your phone number).

To all of the rest of my family and friends, thank you for putting up with my neglecting our relationships the past few months. To my beautiful girlfriend Alyssa, for all the love and support you showed me during this period. To my dad, for the advice you have given me in this project, throughout college, and throughout my whole life. If you hadn't convinced me that being a doctor was for girls, I would probably be in medical school instead of mechanical engineering. To my lovely mother, homeschool teacher, Cub Scout leader, bible class teacher, band booster, and lunch lady (er… gourmet chef), thank you for putting my needs above your own always. You are the reason for me. I love you Mama.

For all of the wonderful people and blessings in my life, I thank my father God. He deserves all the glory and the entire honor, and I depend on him for every breath.

# NOMENCLATURE

P  Pressure

T  Time

CW  Clockwise

CCW Counter clockwise

DIC  Differential Interference Contrast

NA  Numerical Aperture

SS  Stainless Steel

TA2  Unalloyed Titanium Grade 2

# TABLE OF CONTENTS

**LIST OF FIGURES**

Page

xii

# LIST OF TABLES

**CHAPTER I**

**INTRODUCTION**

This chapter provides background information that will be useful for understanding the thought processes and the actions performed in this experiment. The section deals with two major realms of understanding: the use and implementation of bio implant materials and the properties and the multifaceted properties of metals on different scales and for different functions.

Knowledge of internal fixation is crucial to understanding the objectives of this research. The implants examined are all internal fixation devices, so understanding their function and environment explains the conditions to which they have been exposed.

The first division of this section deals with the process of internal fixation. The history is described, as well as the numerous types and methods along with their uses. The biological process of bone healing during the fixation process is elaborated upon, along with the benefits to the healing process for using internal fixation. Some common materials used in these applications are discussed. Finally, the different causes of failure of the bone fixation are examined.

The second division of this section investigates the different ways that a doctor can label the implant as a failure, and the methods by which an engineer can understand this failure on the mechanical property level. The failure criteria discussed are bending, fatigue fracture, and negative response from the human body. The principles and properties that govern these criteria are looked at in depth.

## 1.1. Internal Fixation

Internal fixation is an innovation that orthopedic surgeons have named one of the most significant advances in treatment. This treatment has shortened hospital stays, caused bone to heal faster, and reduced the number of instances where the bone heals in an improper position [1].

### 1.1.1. History of Internal Fixation

Before the use of internal fixation, fractures were generally treated with splints, casts, and braces. Fractures that resulted in soft tissue damage usually called for amputation, notably during the Civil War [1]. Lister first introduced open reduction internal fixation for the patella in 1860. In the 1880s and 1890s, the use of plates, screws, and wires was first documented. Danis and Muller refined the process of internal fixation in the 1950s, and contemporary techniques have been established within the last 40 years.

### 1.1.2. Types of Internal Fixation

Some common devices used in internal fixation are wires, plates, nails, screws, rods, and pins [1]. Wires are generally used for small fractures or in conjunction with other internal fixation methods. An example of wire internal fixation is shown in Figure 1.

Figure 1. Internal fixation of a fractured elbow using wires [2].

Plates are used to fix two pieces of bones that have detached during fracture. The plate holds the two pieces together with screws on either side. Rods and intramedullary nails are used in some fractures of long bones to fit inside the bone where the marrow would have been. Screws are applied from the outside of the bone to connect through screw holes in the rod or nail. The screws can be loosened to adjust the load on the bone, but the rod usually stays in the bone unless complications require its removal. Screws can be used on their own to fasten two bone fragments together. Screws are the most common form of bone fixation [1].

### 1.1.3. Biology of Fracture Repair

The body's natural fracture repair follows a four-step process. This process is illustrated in Figure 2.
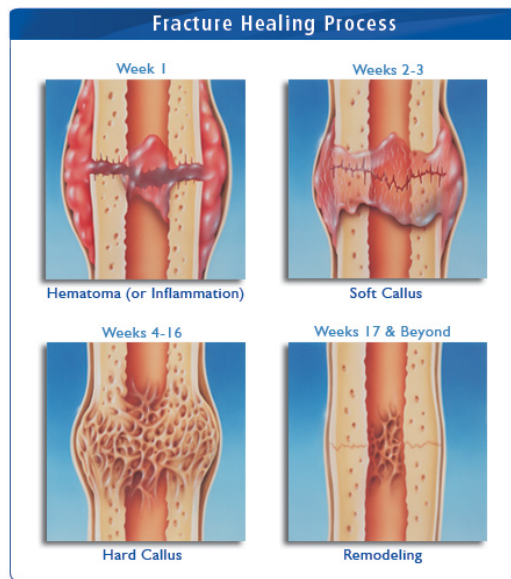
Figure 2. This figure illustrates the fracture healing process.

The first phase of fracture repair that occurs is inflammation. The ends of the damaged bone bleed and form a clot, and polymorphs, histiocytes, and mast cells begin the process of cleaning up. The next phase is the periosteum or soft callus stage, where cell division occurs and forms a callus around the dead ends of the bone. The soft callus is slowly replaced by hard callus to provide solid structure. Once the callus has connected the fracture, the remodeling phase occurs. The callus bone tissue is replaced with osteoclasts and osteoblasts to form the original cortical/cancellous bone structure [3].

With proper fixation, strain is greatly reduced at the fracture site and the bone can heal without forming a callus. This is called direct bone healing. Osteons bond the

portion of bone that is in contact, and membranous bone fills the gaps where the bone

fragments do not contact -- this is replaced by cortical and cancellous bone later. Direct

bone healing greatly reduces the healing time [4].

### 1.1.4. Materials Used in Internal Fixation

Materials in internal fixation applications are subject to many criteria. They must

have high yield strength, elastic modulus similar to that of bone, low density, anti-

corrosive properties, and cannot cause allergy or reaction in the human body. These

strenuous standards limit the known materials that can be used for internal fixation.

Materials operating in the human body must be both "biofunctional" and

"biocompatible". Biofunctionality describes the ability of the metal to perform all of its

functions while inside the human body. Biocompatibility confirms the material is

compatible with the human body. Three main materials have been used in the recent

history of internal fixation: titanium, stainless steel, and cobalt chromium alloy. Data for

these bio-implanting metals from literature findings are compiled in Table 1.

Table 1. This table characterizes some commonly used bio implant
metals [5].

| Materials | Use | Limitations |
|---|---|---|
| Pure Titanium | Most internal fixation | Almost no limitations |
| Alloyed Titanium | | |
| Stainless Steel | Intramedullary nails | Susceptible to corrosion |
| Cobalt | Hip arthroplasty | Slight corrosion, weak mech. |

#### 1.1.4.1. **Resistance to Corrosion**

In order to maintain its mechanical properties in the human body environment, a material must have corrosion resistant properties. The saline solution in the human body serves as an excellent electrolyte for metal ions to diffuse from the metal's surface in an electrochemical reaction. This presents difficulties, as even more care must be taken to ensure the anti-corrosive properties than in a normal working environment. The human body also contains molecular tissue species to combat foreign objects in the body, and biochemical attacks would facilitate a reaction to break down any strange objects in the body. Of the three examined materials, titanium has the highest corrosion resistance [6]. Cobalt chromium also remains fairly passive, but stainless steel can be susceptible to film breakdown and corrosion [5, 7].

#### 1.1.4.2. **Tissue Response to Materials**

Even though stainless steel, titanium, and cobalt chromium are classified as biocompatible, the tissue still responds negatively to corrosion products from these

materials. Stainless steel corrodes more than cobalt chromium and titanium, and the severe cases can cause inflammation and even infection to the point that the implant must be removed. Titanium corrosion occurs in small amounts, and the resulting particles are rarely harmful or painful to the patient [8]. Thick fibrosis layers form for around stainless steel and cobalt chromium, sometimes up to 2mm. Minimum fibrosis formation is observed for titanium [5]. These fibrosis layers wall off the living tissue from the foreign object, but bacteria multiplies in the absence of antibodies.

1.1.5. **Common Causes of Failure**

While the research in this paper investigates an alteration in mechanical properties as a cause of failure, many other factors often contribute to a failure. The three main categories of reasons for failure are a defect in the fixation device, an incorrect implanting procedure, or extraneous patient based factors that were not taken into consideration. Seldom can one of these reasons take 100% of the blame as multiple factors always contribute. These factors can never be eliminated – only reduced.

1.1.5.1. **Fixation Device Defect**

The factors that engineers can directly control are those related to device design. Internal fixation devices need to be designed to reduce stress concentration geometries, and to be biocompatible. Stress concentrations are manifested at screw holes, changes in cross sectional area, and bends in the axis [9]. Extensive research and trials over time have produced the optimal biocompatible materials, but the right material must be chosen for the application. When the material is not designed properly in terms of geometry or material, the fixation assembly is exposed to a high risk of failure under

normal circumstances. The part can also be manufactured incorrectly, or damaged due to negligence before fixation occurs. When deviation occurs at the fixation device, this factor can lead to failure in the implant or bone fixation.

### 1.1.5.2. **Incorrect Medical Operation**

Another factor that leads to failure of an internal fixation is the improper implementation by the medical professional. Many problems can arise during the fixation process, complicated by the fracture pattern [10]. Channels can be drilled in incorrect locations, incorrect screw length can be used, or screws can be over tightened [11]. The correct tools must be used for each operation, and the proper sanitation must be upheld to prevent infection. The subjectivity of this area places a burden on the doctor to perform with an alert and risk-averse mindset. Because the fixation method relies on the doctor's opinion, this operation is not an exact science and is a viable factor in any fixation failure.

### 1.1.5.3. **Patient Factors**

Besides problems with the implant or the medical procedure, the problem can rest on the individual receiving the fixation. The mechanical properties of the bone are different for every person, so every fixation must include a safety factor to account for this [12]. The sizes of implants are different to account for the anthropometry of the current population.

The patient can also be a factor in the success of the fixation by cooperating with the doctor's orders. Placing load on a fixation too early can complicate healing or even cause the fixation device to fail. Engaging in certain physical activities is prohibited in

many cases following fixation, so the bone can have some time to heal. Failure to follow

the doctor's prescription is a prevalent factor in internal fixation failure.

Accidents are a major cause of fixation failure. Not all incidents can be

prevented, and disasters lead to broken bone or implants often. Falls, car accidents, and

sporting injuries are all examples of physical traumas that complicate fixation healing.

A patient may have physiological or pathological conditions that affect the

healing of the bone fixation. Osteoporosis is the most common condition that affects

bones. Osteoporosis causes a decrease in bone density and mass, as seen in Figure 3

[13].
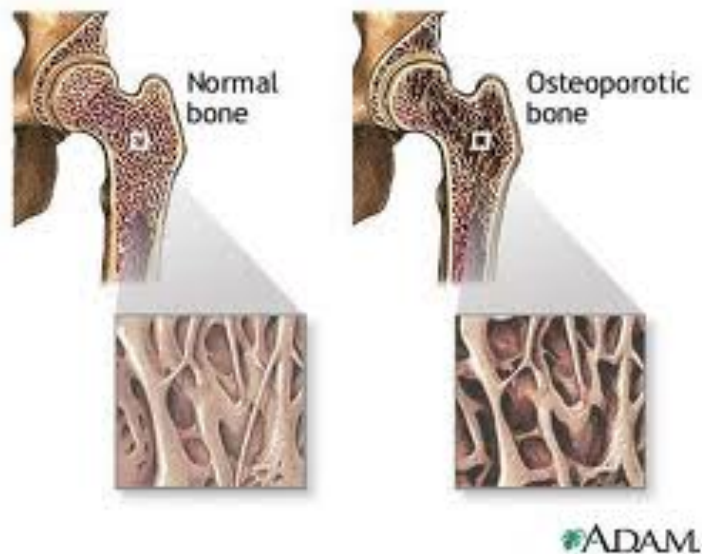


Figure 3. Normal bone versus osteoporotic bone shows the change in
structure and density [14].

This condition presents a real danger to many people. Decreasing the mechanical properties greatly increases the chance of fracture, and can also lead to complications after bone fixation. The bone may not be able to bear load like a normal bone, or screws may strip the bone [15]. Other disorders like osteopenia, osteomalacia, and hyperparathyroidism can also cause weakness in the bone that can compound with other complications to cause a failure in the bone fixation. Bone density is found to correlate directly with fracture stability [16].

## 1.2. Diagnosis and Evaluation of Internal Fixation Devices

There are many criteria by which an engineer may evaluate the ability to succeed of an internal fixation device. A doctor may diagnose the failure of an implant by looking at an x-ray image, but an engineer looks at the mechanical properties of the material to determine its performance quality. This section introduces the methods by which a problem with an implant may be diagnosed and evaluated.

### 1.2.1. Bending

The patient can usually diagnose the failure as well as the doctor can in the case of bending. The implant can bend for a variety of reasons such as under-designed structure from the engineer, incorrect prognosis by the doctor, or by overloading from the patient. The post-failure evaluation explores the mechanical properties of the material to decide how the implant was insufficient and how it can be improved. (Spoiler alert) During an evaluation, the engineer may discover that the metal does not have the same properties it once had. In the case of bending, two mechanical properties are

examined that relate to the failure: yield strength and elastic modulus. It is important to

remember that in bending, the highest stresses accumulate at the surface [17]. Thus a

surface evaluation is a great indicator for analyzing an implant.

### 1.2.1.1. **Yield Strength**

The yield strength of a material is the point at which the material begins to

undergo plastic deformation. Before this strength is reached, the material is governed by

elastic deformation. After the material has exceeded its yield strength, the elastic

deformation can be recovered while the plastic deformation cannot [18]. A typical stress

strain relationship is shown in Figure 4.
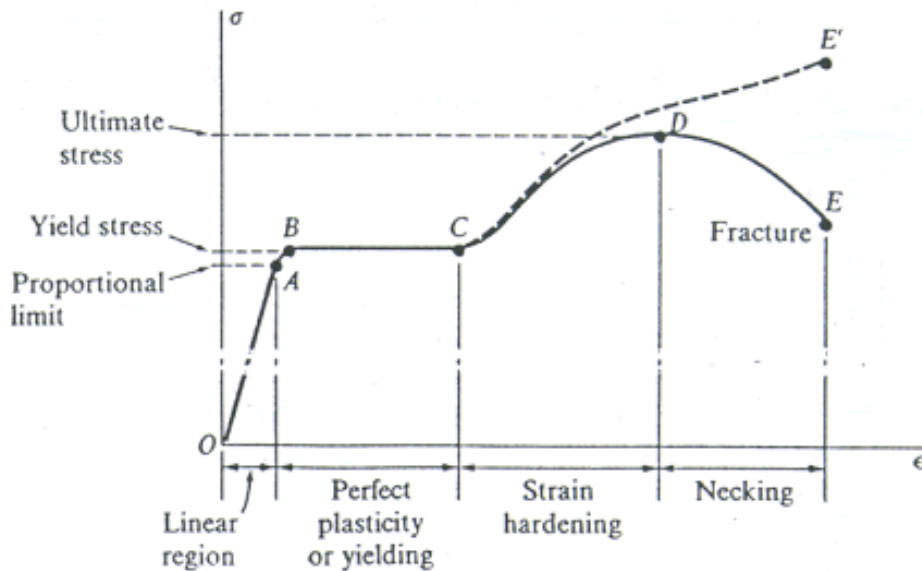


Figure 4. The stress strain curve shows extensive deformation once the
yield stress (or strength) has been reached. The material is AISI 4140
alloy steel [18].

In most internal fixation device failures the implant yields, which also complicates the bone healing. Implants are designed so that the expected loads fall far below the material's yield strength.

### 1.2.1.1.1.  Relation to Hardness

To test the yield strength without machining tabs from the implant to tensile test, hardness testing can be used to evaluate the yield strength [19]. An equation from experimental data can be used to model the relationship, which has been proven to be linear for many metals. The equation used for steels is

$$YS = \frac{H}{3} B^n \qquad (1.1)$$

where YS is the yield strength, H is the hardness, B is a constant 0.1 for steels, and n is the strain hardening exponent [20].

### 1.2.1.1.2.  Relation to Microstructure

A microstructural analysis can provide insight towards the yield strength of a material. The grain size has been shown to affect the material properties. Yield stress is related to the grain size by the Hall Petch relationship

$$S_y = S_0 + k_y D_{GB}^{-\frac{1}{2}} \qquad (1.2)$$

where sy is the yield stress, s0 is a material constant for the resistance to dislocation motion of the lattice, ky is the strengthening coefficient of the material, and d is the average diameter of the grains. By examining the size of the grains under a microscope, one can approximate the yield strength of the material by the Hall Petch relationship shown above [21].

Any yield or plastic deformation is unacceptable according to the design of internal fixation devices. Although the material may not have fractured at this point, additional stress will cause the material to rapidly fail.

### 1.2.1.2. **Wear Resistance**

Wear resistance is an indirect measure of a material's strength at the surface level. Whereas yield strength quantifies the strength under tension or other conventional loading patterns, wear describes a material's ability to resist plastic deformation as the result of a sliding or frictional force. There are numerous wear mechanisms that fall under this category.

One type of wear is adhesive wear, in which material is transferred from one surface to another during sliding contact. This type of wear is dependent on the roughness of the materials, as it often occurs when the peaks of a rough surface plastically deform and attach to the contact surface. Galling is one effect of this type of wear, when material builds up and forms lumps above the original surface line [22].

Abrasive wear occurs when a harder and rougher surface slides against a softer and smoother one. Material is removed from the softer surface due to scratches from the hard material. A few different mechanisms occur during abrasive wear: plowing, cutting,

and fragmentation. Plowing involves material moving to the side of protrusions from the hard surface and forming scratches or valleys. The material is not removed but displaced. Cutting can be compared to machining, where material is chipped or cut away without significant displacement or deformation of material on the surface. Fragmentation occurs during cutting when the abrasive process deforms the material surrounding the removed portion, and cracks propagate through the remaining wear material [23].

Surface fatigue wear occurs when the surface has been stressed in cyclic loading to the point that micro-cracks have formed and material begins to deteriorate and detach [24]. Fretting wear happens in a similar process, where two surfaces are rubbed together cyclically [25]. Material may be removed from one or both surfaces in this process.

Erosive wear appears when solid or liquid particles are passed over a surface until material from the surface detaches or erodes. The rate of this type of wear depends on the size, shape, hardness, and speed of the particles [26].

### 1.2.2. Breaks or Cracks

When the implant fails completely by fracture, the bone is in danger of bearing the entire load imposed by the human body. Depending on the stage of bone healing, the bone may also re-fracture or not heal. Cracks are less consequential, but have the possibility of propagating and eventually causing a fracture [9]. These types of failure are generally produced by two factors: fatigue and incorrect placement. These two factors are not mutually exclusive, and often compound on each other to cause a fracture.

### 1.2.2.1. **Fatigue**

Fatigue is a failure that occurs when a material has been subjected to cyclic loading. When a material experiences loads above a certain amount, micro-cracks form in the material. If these loads are repeated enough, the micro-cracks expand and propagate, leading to a sudden fracture [27]. In metals, cyclic loading causes dislocations to move and interfere. When dislocations meet, localized hardening and brittleness occurs in the material. This encourages cracking in the material [28].

One important thing to note is that damage from fatigue is cumulative. Even after the material rests from cyclic loading, the damage will not recover even though the deformation is elastic. If the cyclic stress is low enough, the material can theoretically survive for an infinite amount of cycles. This is often exhibited in metals like steel and titanium. Fatigue life is also affected by a variety of parameters, including temperature, surface finish, microstructure, oxidizing chemicals, and residual stresses.

Loading and unloading occurs in any internal fixation implant as the patient walks and goes through their daily activity. The materials are selected so that the cyclic loading will be below the fatigue limit, allowing the implant to theoretically survive and outlive the patient. However, if the cyclic loading is too high or if the parameters affecting the fatigue life are changed too drastically, the implant still has a risk of failure.

Stress concentrations because of geometry increase the probability of fatigue failure. For internal fixation, screw holes are the primary candidates for stress concentrations [29]. Interlocking screw fixation especially increases the stress at the screw holes, but sometimes has its benefits. Studies have shown that in some cases,

15

interlocking screws are necessary to prevent mal-union or limb shortening [30]. For most

cases, however, dynamic fixation is suggested to reduce stress concentrations. Dynamic

fixation includes one screw hole that functions more as a slit, allowing the screw to be

loosened and slide to release stresses applied by shifts in the fixation [15].

1.2.2.2. **Incorrect Placement**

Incorrect placement of the implant can cause fracture when the geometrical stress

risers in the implant align with the high stress areas of the fracture. Figure 5 shows a

femoral intramedullary nail fixation where the proximal interlocking screw was placed

in proximity to the fracture site, and directly on top of an area of bone deformation.



Figure 5. An x-ray image of a femoral fixation shows that in
intramedullary nail has failed. The screw was placed close to the
fracture and bend in the bone.

When an implant is placed incorrectly, it usually compounds with fatigue for a low cycle failure. The doctor should correct abnormalities or weaknesses in the bone before fixing an implant to that area. If the screw holes naturally fall too close to the fracture area, a different type of implant or in this case a longer intramedullary nail could be used.

### 1.2.3. Negative Reaction by the Human Body

Even if the implant does fine, the fixation can still be considered a failure due to the effects it has on the human body. Assuming that a biocompatible material has been chosen, complications can still arise within the fixation. Sometimes, the bone does not heal despite the proper fixation assembly. The surrounding tissue is subject to infection and inflammation due to the metal or improper sanitation.

#### 1.2.3.1. Failure to Heal

When the bone does not connect after ample amount of time post fixation, a mal-union has occurred. Mal-union has also been discussed for improper placement, as the bone is not properly aligned [31]. Nonunion occurs when the bone does not connect completely or at all [32]. Figure 6 shows an example of malunion and nonunion.
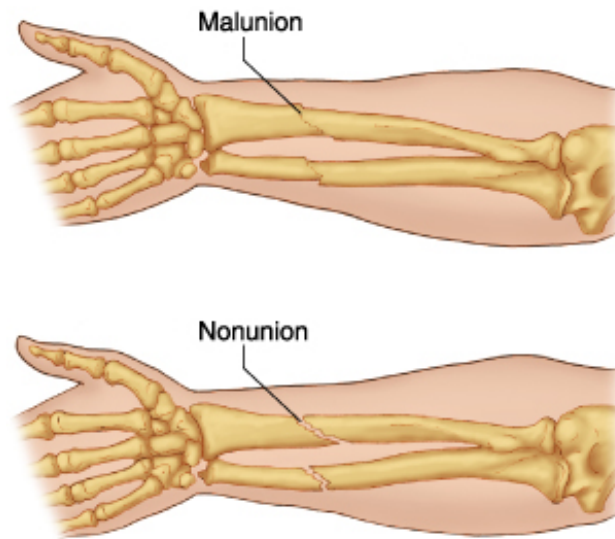
Figure 6. Malunion is a misalignment while nonunion occurs when the
bone does not heal [33].

### 1.2.3.2.  **Infection or Inflammation**

Infection occurs when there is an imbalance of the body's defense system and
infectious bacteria. The body's defense mechanisms are weakened by the trauma of the
initial fracture, the surgical operation and fixation, and also by the addition of a foreign
object into the body [34]. Infection is linked to nonunion and mal-union, and the implant
is almost always removed in this case [35]. Figure 7 shows an example of an infected
internal fixation.

Figure 7. An infected internal fixation. Plates and cables are attached to
a dead tibia with infected tissue surrounding [36].

Inflammation is connected to infection, but does not always indicate a bacterial attack. In surgical implants, metal fragments that have come loose from wear or corrosion can irritate the human tissue. This type of inflammation (excluding the case of bacterial infection) can usually be ignored, as it does not halt the healing process [37].

# CHAPTER II

## MOTIVATION AND OBJECTIVES

As discussed in Chapter 1, implants fail for a variety of reasons. Extensive research has been performed on the biocompatibility of metals used in bone fixation implants, but little efforts were made in understanding effects of the human body on the materials. If the mechanical properties of metals used for internal fixation do change while in the human body, additional design considerations will be required. This research focuses on evaluating mechanical and surface properties of materials that have been removed after being implanted in the human body. The three objectives are as follows:

- Locate high-stress areas where the implants might be affected during service using SolidWorks
- Obtain quantitative evaluation of material properties before and after implantation
- Obtain understanding in effects of human body on materials before and after implantation

The primary research involves experimental approaches. The sections of study are morphological evaluation, corrosion potential analysis, and mechanical property measurements. A simulation of the stress distribution in the human femur is included in the next chapter.

The simulation models the femur in two cases: normal stresses during walking and stresses during a car accident. The simulation served to identify high stress locations

20

on the femur so implants in that region can be studied. Followed by the examination of surface morphology and their resulting microstructure. Mechanical behavior of samples was compared before and after implantation. The outcome of this research will have impacts on the design considerations for bone fixation implants. If the mechanical properties of metals change while in the body, then different materials may be selected, or the parameters of the implants may be enhanced to account for degradation.

## CHAPTER III

## FEMORAL STRESS DISTRIBUTION

In terms of bone injury, the fracture of the femur is one of the most common and consequential. The femur is the largest and strongest bone in the body, but can weaken greatly as a person grows older. The density and strength of the femur can be lowered by osteoporosis, osteopenia (low bone density), osteomalacia (lack of vitamin D), and hyperparathyroidism (delegation of calcium to other parts leading to a deficiency. In the United States, 44 million people have osteoporosis or low bone mass, which represents 55% of the population 50 or older. Although less important than human life, medical costs are approximated at $40,000 for every hip fracture [38].

The importance of this chapter is to show the locations of stress concentrations on the femur to understand the locations in which fixations and implants can expect to experience the highest stresses. The fracture does not always occur at these locations, due to accidents where the forces are applied in unpredictable fashions. However, the simulation using the finite element method will help to understand the stress distribution on the bone and on implants during loading.

### 3.1. Femur Model and Test Simulations

Average mechanical properties were tabulated for the human femur, and the values appear in Table 2.

Table 2. This table lists the average mechanical properties found for the human femur [39].

| Properties | Values | Units |
|---|---|---|
| Elastic Modulus | 1.7E+10 | N/m^2 |
| Shear Modulus | 7E+9 | N/m^2 |
| Mass Density | 1500 | kg/m^3 |
| Tensile Strength | 1.3E+8 | N/m^2 |
| Compressive Strength | 1.9E+8 | N/m^2 |
| Yield Strength | 1.0E+8 | N/m^2 |

These properties were used with a solid model of a femur generated by Redding Engineering LLC from a bone scan. For stress analysis, models in Solidworks require both dimensions and material properties. The properties were added to the model in Solidworks. The model used in this simulation appears in Figure 8.
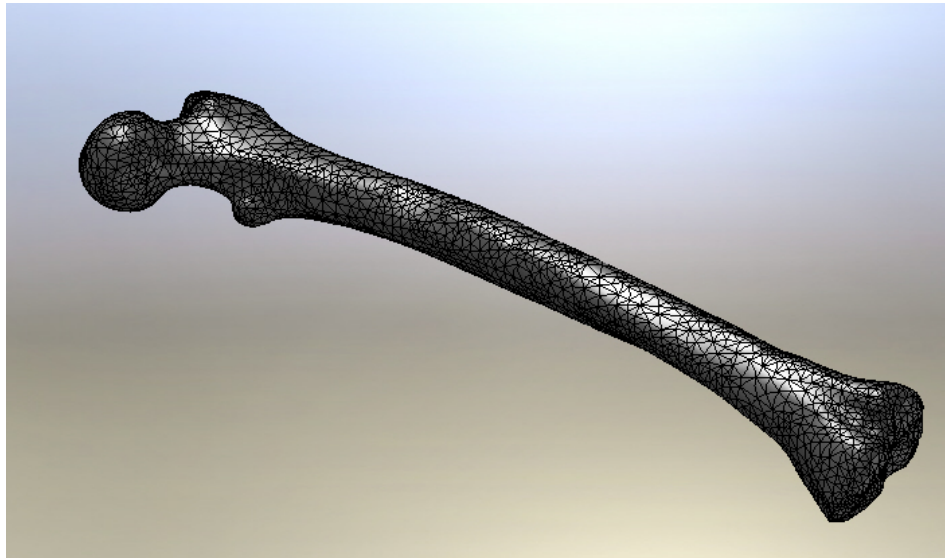


Figure 8. The Solidworks femur model was created from the bone scan of a real human femur.

The simulation was conducted using the SimulationXpress package in the Solidworks software. As seen in the figure above, the model was meshed into many smaller pieces. SimulationXpress uses the finite element method, which divides the model into many smaller elements to solve the stress distribution. The stresses (or strains and displacements) are calculated at the nodes of the elements. Using finite element analysis, the linear static assumption was also made – this assumes small displacements, small rotations, linear elastic materials, and constant boundary conditions [40].

Two test conditions were chosen: one for a femur under normal stresses during walking, and one for a traumatic car accident. The initial conditions required that fixtures and forces be applied to the model. The test conditions are shown in Figure 9.
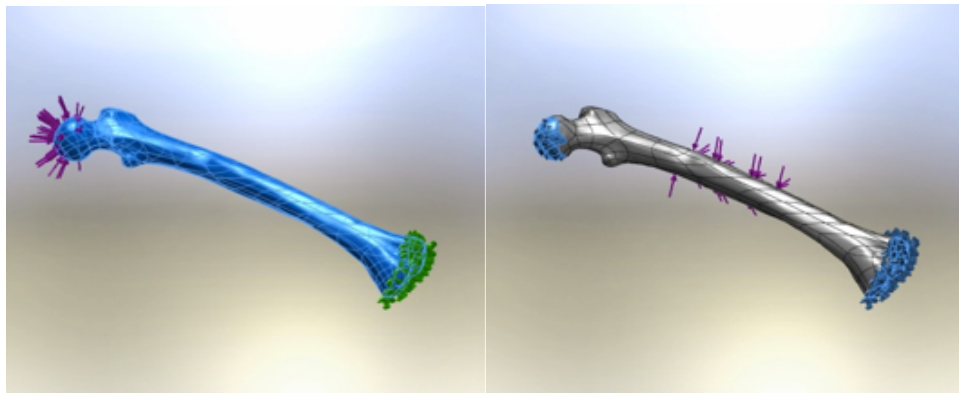


Figure 9. The Solidworks stress analysis required both fixtures and forces for each simulation: walking (left) and car accident (right).

As is seen in the figure, the simulation for the walking case included fixture at the condyle region of the bone (the green area) and applied force at the head (the purple arrows). The total force to the head was the force that the average person applies during walking, 2100 N [41]. The car accident case had fixtures at both ends and the force being applied at the shaft. This accident could never be perfectly predicted or simulated but a worst-case scenario was constructed for the force being applied normal to the shaft at the center. 15 kN were used at the shaft to model the car accident [42].

## 3.2.  Stress, Strain, and Displacement

The results for the stress, strain, and displacement distributions were simulated, and the results are shown in Figure 10, Figure 11, and Figure 12.
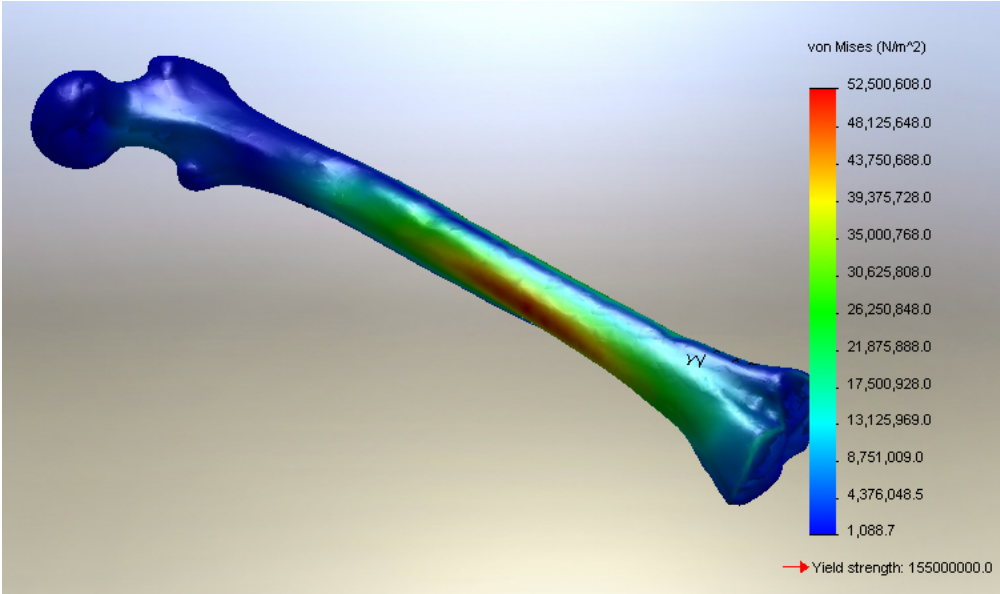


Hki wtg"320"Vj g'uvtguu"cpcn{uku'uj qy gf "c"eqpegpvtcvkqp"qp"yj g'uj chv"hqt
"y cmkpi "*cdqxg+"cpf "c"eqpegpvtcvkqp"qp"yj g'pgem"hqt "cp"ceekf gpv"*dgmqy +0

25

Figure 10: Continued
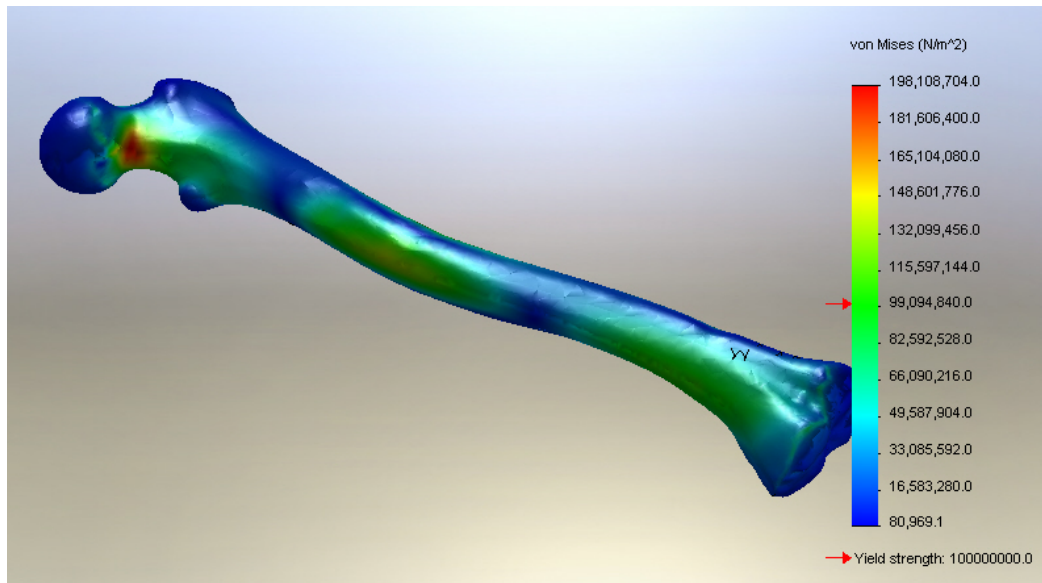
For the walking case, the highest stress (shown in red) was focused on the shaft. The highest stress does not come close to the yield stress, and the femur is never expected to fail during static loading during walking. In fact, the walking case more closely would follow a fatigue failure. Since the bone has the ability to heal, fatigue failure is unlikely in the human bone - but these data still have meaning for an implant inside the bone at that region. The highest stress in the walking case was 52.5 MPa. In the car accident case the highest stress (shown in red) was located at the neck. A fracture in this area would be classified as a hip fracture. In elderly people, over 90% of hip fractures are the result of a traumatic accident like a fall [43]. The car accident case certainly does not model every accident, but non-axial loading is shown to produce

stresses at the neck. This agrees with the hip fracture/accident correlation. For the car accident case, the yield stress is exceeded as seen on the scale bar. The highest experienced stress was 198.1 MPa. Since stress and strain are related due to the elastic assumption, the distribution was identical with different values on the scale bar. The walking case showed the highest strain on the shaft, and the car accident case showed the highest strain at the neck. The highest strain for the walking case was 0.00139 (unit less) and the highest strain for the car accident was 0.00789 (unit less).
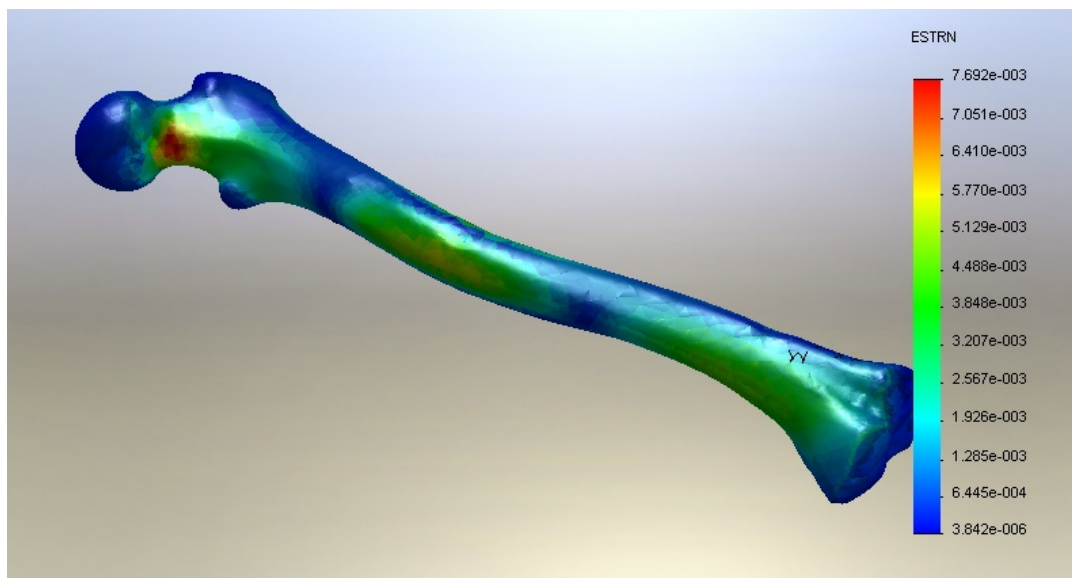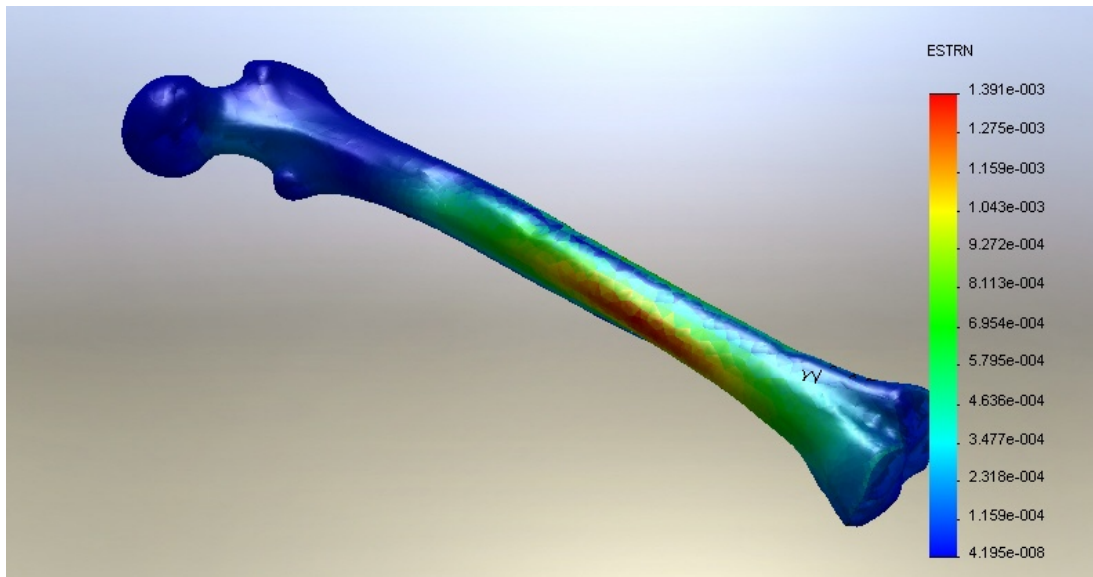
Figure 11. The strain analysis showed essentially the same distribution
as the stress analysis.
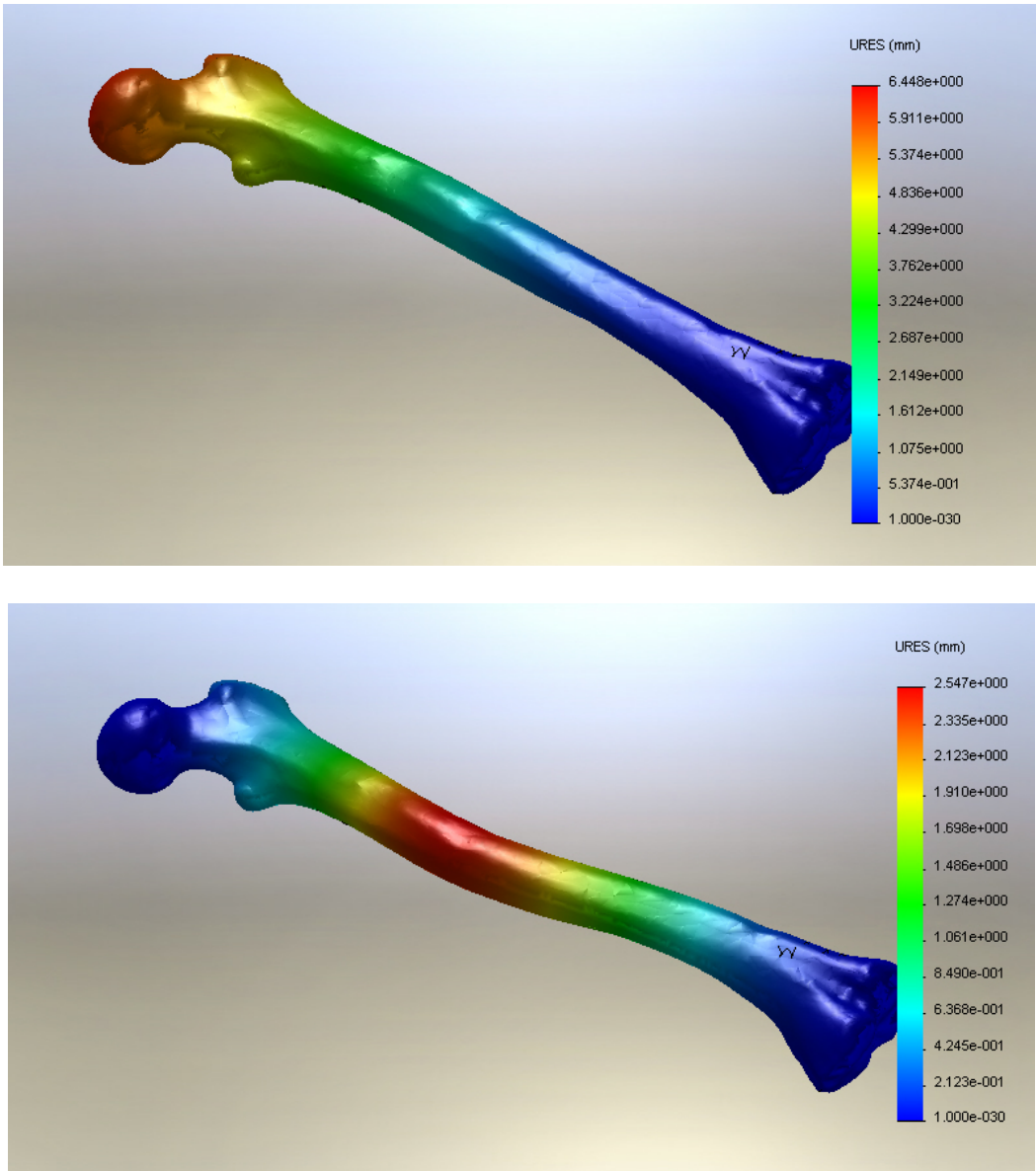
Figure 12. The displacement analysis showed the head deflecting for
walking (above) and the shaft deflecting for an accident (below).

The displacement map exaggerates the expected deformation pattern for the
simulation. The walking case shows that the head has deflected the most – away from
the fixed condyle region. The maximum displacement is 6.4 mm, which is not dangerous

for a flexible single cantilever bending system. The car accident simulation is closely described as a double cantilever, where both ends are fixed and not allowed to rotate. The maximum displacement of 2.5 mm occurs at the shaft, which explains the large stresses near the fixture points that cannot rotate with the force.

### 3.3.  Remarks

The two cases simulated in Solidworks show the regions of the femur that can expect to experience the highest stresses (cyclic and sudden), strains, and displacements. Understanding the mechanical conditions affecting the femur is beneficial in understanding the conditions that implants can expect to face – especially implants designed for those high risk regions. Bone fixation devices that mend the neck of the femur or the middle of the shaft are in regions of high stress, strain, and displacement. The materials to be examined later in this paper are stainless steel and titanium. The yield strengths of the specific alloys are listed in Table 3 along with the yield strength of the femur (this value is the same average value used in the simulations). These values can be compared with the maximum stress of 52.5 MPa for walking and 198.1 MPa for a car accident.

Table 3. This table lists the yield strengths of the materials to be
examined and also the femur.

| Material | Yield Strength (MPa) |
|---|---|
| Stainless Steel 316L | 170 |
| Unalloyed Titanium Grade 2 | 275 |
| Femur | 100 |

Given the test conditions, all of the materials would have withstood the walking

case (as expected) but only the titanium would survive the stresses induced by the car

accident. Understandably, the stresses on the femur are not exactly what the implants

would experience, but they do provide an estimate for what the implants could expect.

This mechanical risk along with the biochemical factors of fixation can compound to

cause complicated failures as seen in the introduction chapter. This simulation highlights

the importance of studying implants used in these high stress locations.

# CHAPTER IV

## EXPERIMENTS

This chapter discusses the experimentation performed in response to the question of degradation in the bone implants. The goal is to compare the properties and performance of implants before and after implantation leading to understanding of their failure mechanisms.

The tested materials will first be examined, and the standard properties will be referenced in the experimental results. This section contains information pertaining to chemical composition, mechanical properties, crystal structure, phase, and other material properties.

The sample preparation will be fully defined along with notation and schematics relating to the position of measurements, the direction measurements are to be taken, and the physical preparation of the samples for experimentation.

The experiments will be discussed theoretically and procedurally. The equipment will be listed and described. The theory and reason for choice behind each experimental method will be explained.

## 4.1. Materials

The materials tested in this experiment were donated by the Shandon Province Hospital in China. The hospital provided implants that had failed inside the human body and then been removed. The hospital also provided identical implants that had never been used as control samples to see the effects of the human body.

### 4.1.1. **History of Implants Studied**

Four sets of implants were tested, and a set comprises an implanted sample and its control. Of the four sets, three were stainless steel 316L and one was unalloyed titanium grade 2. All of the stainless steel implants were intramedullary nails while the titanium implant was a femoral plate. Two of the stainless steel implants were designed for the femur and the other was designed for the tibia. Pictures of the implants are shown in Figure 13.



Figure 13. The tested samples supplied by the Shandon Hospital in order from top to bottom: long femoral nail, short femoral nail, tibial nail, femoral plate.

### 4.1.2. **Materials**

The materials to be examined in this section are biocompatible and highly corrosion resistant because of their use in the human body. Stainless steel 316L and

commercially pure Titanium TA2 are the materials used in the implants that were tested.

These materials are common structural biomechanical materials because of their non-

harmful natures to the human body, and their high strength to weight ratios [7]. A list of

selected mechanical properties for these alloys is compiled in Table 4.

Table 4. This table lists some of the basic mechanical properties of
stainless steel 316L and commercially pure titanium alloy 2 [44-46].

| Mechanical Property | SS 316L | TA2 |
|---|---|---|
| Young's Modulus [GPa] | 193 | 116 |
| Yield Strength [MPa] | 170 | 275 |
| Density [g/cm^3] | 8.000 | 4.506 |
| Strength to Weight [Nm/kg] | 254 | 288 |

### 4.1.3.  **Stainless Steel 316L**

Stainless steel 316L alloy is commonly referred to as surgical steel for its use in

bone fixation screws, prostheses, and body piercings [47]. The elements and

composition for stainless steel 316L are listed in Table 5.

Table 5. This table describes the chemical composition of stainless steel
alloy 316l [48].

| Element | Composition [%] |
|---|---|
|  |  |

| | |
|---|---|
| Iron | Balance |
| Carbon | <0.03 |
| Chromium | 16-18 |
| Nickel | 14 |
| Molybdenum | 2-3 |
| Manganese | 2 |
| Silicon | 0.75 |
| Phosphorus | 0.045 |
| Sulfur | 0.03 |
| Nitrogen | 0.10 |

The intramedullary nails examined in this paper are all made of austenitic 316L stainless steel. Steel is used over Titanium in some cases of bone fixation because of cost considerations, but Titanium is less corrosive, stronger in terms of yield and tensile strength, and much lighter.

### 4.1.4. Commercially Pure Titanium Alloy Grade 2

The elements and composition for commercially pure Titanium Alloy Grade 2 are listed in Table 6.

Table 6. This table describes the chemical composition of
commercially pure titanium alloy grade 2 [49].

| Element | Composition [%] |
|---------|-----------------|
| Titanium | 99.67 |
| Carbon | 0.08 |
| Iron | 0.3 |
| Nitrogen | 0.03 |
| Oxygen | 0.25 |
| Hydrogen | 0.015 |

## 4.2. Sample Preparation

The experiments focused on four sets of implants. Table 7 summarizes these implants and some of the physical characteristics.

Table 7. This table lists the bone fixation samples examined in this
experiment. The material, use, failure mode, and an image are shown
for each of the implants.

| Implant | Material | Use | Failure Mode | Picture |
|---|---|---|---|---|
| Femoral Nail (Long) | SS 316L | Internal Bone Fixation | Bending | |
| Femoral Nail (Short) | SS 316L | Internal Bone Fixation | Fracture | |
| Tibial Nail | SS 316L | Internal Bone Fixation | Fracture | |
| Femoral Plate | TA2 | Exterior Bone Fixation | Fracture | |

The samples to be examined were mounted on a 2x4 wooden pallet on a bed of clay

about 0.5 inches thick. This setup was optimal for exposing a horizontal test surface

without having to use clamps or other potential surface damaging devices. The clay

deformation during testing was deemed negligible, considering the amount of force

required to press the samples into the clay. The long femoral nails are shown in the bed

of clay in Figure 14.



Figure 14. The implant samples were placed in a bed of clay for testing.

A common measurement metric was applied for axial measurements. A mark

was made with a Sharpie marker every inch, starting with the screw holes at the tapered

end (they are exactly one inch apart). Hardness measurements and roughness average

data were taken toward the tapered end in the case of repeated measurements. This

information is included merely for consistency of measurement. A diagram is shown in

Figure 15 to illustrate the measurement designations.
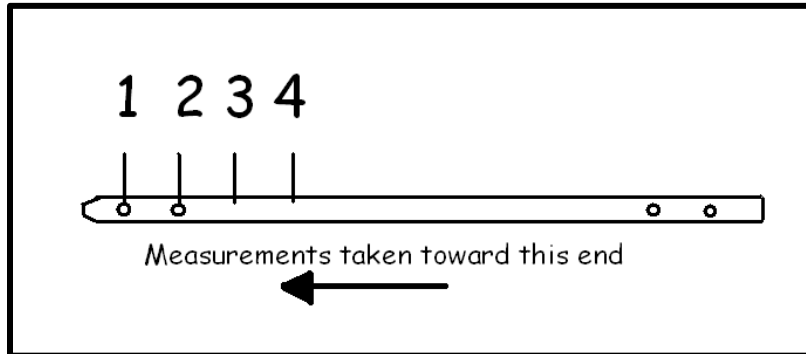


Figure 15. This illustration demonstrates the pattern for taking
measurements for the experiments. For example, measurements taken
at the first inch marking were taken to the left of the hole as shown in
this picture.

The experiments in this section primarily deal with an investigation of

mechanical properties on the surface of the material. The first set of experiments set out

to discover if there has been a material degradation as a result of bone implantation. The

second set of experiments set out to explore the mechanisms of this degradation, and

provide some insight into the cause and effect relationship between the human body and

the materials.

### 4.3. Microhardness

The first experiment was to determine the hardness of the materials to see if there

was a significant difference in the mechanical properties of the material pre and post

implant. Microhardness was selected to test only the surface layer of material (on the order of nanometers), as the bulk material was not expected to see any effect from the human body.

### 4.3.1. **LM 300 Series Vicker's Microhardness Indenter**

The machine used in the experiment was the LM 300 series Vicker's Microhardness Indenter, shown in Figure 16. A Vicker's Diamond indentation tip was attached to the indenter. This method was chosen over Knoop because of the low profile indent, which was needed to pack indents close to each other on a single axial ridge of the implant.

Figure 16. The LM 300 series Vicker's microhardness indenter was
used to test the materials' hardness.

The LM 300 was equipped with 3 objectives and an indenter. The indenter was

set to apply 0.3 kg of force and to hold for 13 seconds. The 2.5X and 10X objectives

were primarily used to position the indentation tip over a flat surface, while the 50X

objective was used to find a suitable position to indent – not close to macro surface

defects. The 50X objective was also used to dimension the indents with the help of the micro-measurement tool in the stage.

### 4.3.2. **Vicker's Microhardness**

The indenter measures the hardness by creating a diamond shaped indent that is the same shape no matter the size. The area of the indent is calculated by measuring the diagonals. Figure 17 shows a schematic of the indentation process and the resulting indent.
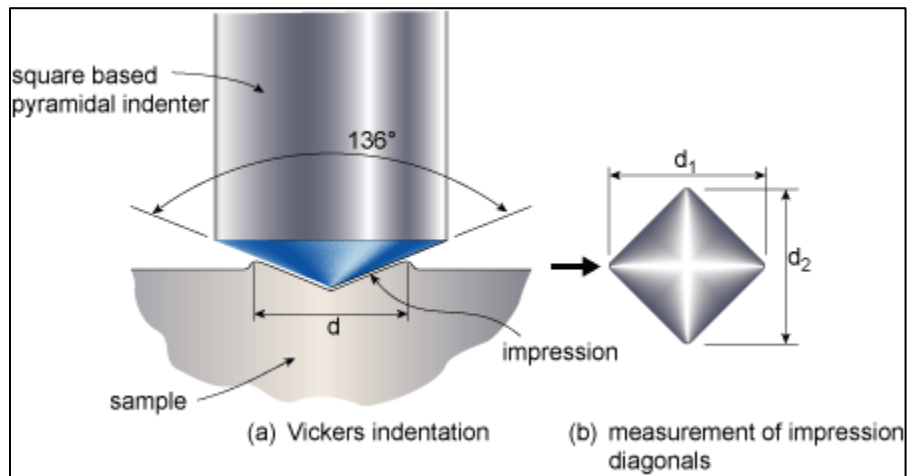


Figure 17. The Vicker's method leaves a diamond shaped indent, which is geometrically similar regardless of size.

The LM 300 computed the Vickers hardness value using the recorded diagonal lengths according to the equations

$$HV = \frac{F}{A} \qquad\qquad (4.1)$$

and

$$A = \frac{d^2}{2\sin(136^\circ / 2)} \qquad\qquad (4.2)$$

where HV is the hardness value, F is the applied force in kg force, A is the area, $d^2$ is the product of the two diagonals, and 136 degrees for the angle of the Vickers indenter [50]. The hardness value is automatically available once the user has manually measured both of the diagonals.

### 4.3.3. **Procedure**

The microhardness indenter requires that a flat surface be exposed for indentation, so the samples were mounted in clay. The clay was firm enough to neglect the deflection during indentation given the small applied load.  A Sharpie marker was used to mark the sample every inch, where separate indentations were performed. Five indentations were performed beside every inch marking, with the indentations spaced apart by approximately 0.1mm. The large number of samples was taken to ensure that an accurate average was derived. Measurements were taken along the entire length of the implant to examine the possible change in hardness along the length due to conditions in the human body. All of the indentations were taken in a line on the ridge where the surface was perpendicular to the indenter. This could be accurately approximated by indenting along a bright stripe where the incoming light was reflected straight back.

43

For the titanium femoral plate, a different method was used. Since the surface was not polished, the Vickers microhardness did not produce meaningful data. Brinnel hardness was used instead just for this sample. The indenter was spherical instead of diamond, but the concept of hardness measurement was the same.

## 4.4. Surface Roughness Evaluation

Roughness is a way to measure the deviation of a surface from the normal form. Many metrics are used, called roughness parameters, to quantify this deviation. If the vertical distances of the variations are high, then the surface is rough. A few of the roughness parameters are described in Table 8.

Table 8. Roughness parameters and the formulas [51].

| Parameter | Name | Formula |
|-----------|------|---------|
| $R_a$ | Roughness Average | $R_a = \dfrac{1}{n}\sum_{i=1}^{n}\lvert y_i \rvert$ |
| $R_q$ | Root Mean Square Roughness | $R_q = \sqrt{\dfrac{1}{n}\sum_{i=1}^{n} y_i^2}$ |
| $R_t$ | Max Peak to Valley Height | $R_t = \max y - \min y$ |

Describing the surface roughness can be useful to predict the performance of the material. Rougher materials tend to wear faster than smooth materials, and defects in the

44

surface create sites for stress concentrations and corrosion to occur. For this reason, an experiment was performed to compare the roughness of the materials pre and post implant.

### 4.4.1. Zygo 3D Optical Surface Profiler

To calculate the roughness parameters, the surface was analyzed using a Zygo 3D Optical Surface Profiler. The Zygo machine uses interferometry to profile the surface. A 10x objective was used for viewing the surface, and a 15 second scan elapsed during the interferometry process. Figure 18 shows the Zygo machine and the test setup.
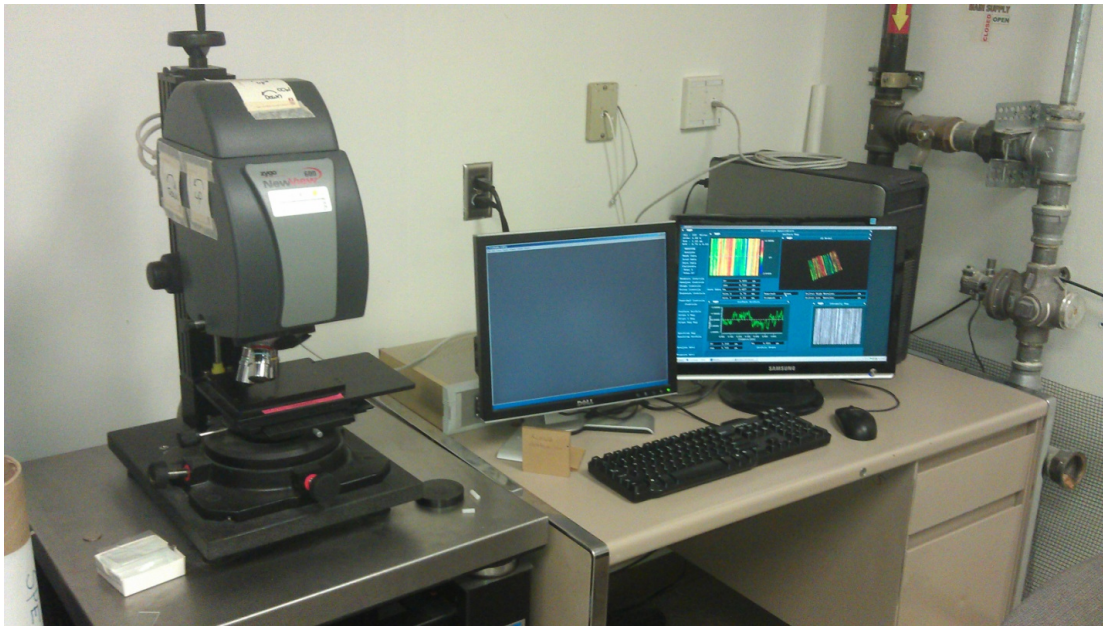


Figure 18. The test setup for roughness measurement includes the Zygo optical profiler, a vibration isolation table, and a computer with software for analysis.

A vibration isolation table was necessary to remove vibrations and noise that would otherwise alter the data. 3D images were constructed and analyzed with the software to produce the roughness statistics for maximum peak to valley height, roughness average, and root mean square roughness average. The roughness average is the most commonly used parameter, and serves our purposes for comparison.

### 4.4.2. **Interferometry**

Interferometry uses the diffraction pattern of light to map the surface that the light has reflected from. A beam splitter creates two beams of light, the original and the incident. The original beam passes through the beam splitter to a CCD camera, while the incident beam expands and passes through a collimator. The incident beam exits the collimator with parallel rays, and passes through a piezo phase shifter. After this the incident beam reflects from the test piece and returns through the piezo phase shifter and the collimator. The two beams are imposed on each other in the CCD camera, and the out of phase beams create a diffraction pattern. From this diffraction pattern, the topography of the surface can be extracted since beams that travelled a farther distance will be out of phase with beams that travelled a shorter distance. Figure 19 illustrates this process.
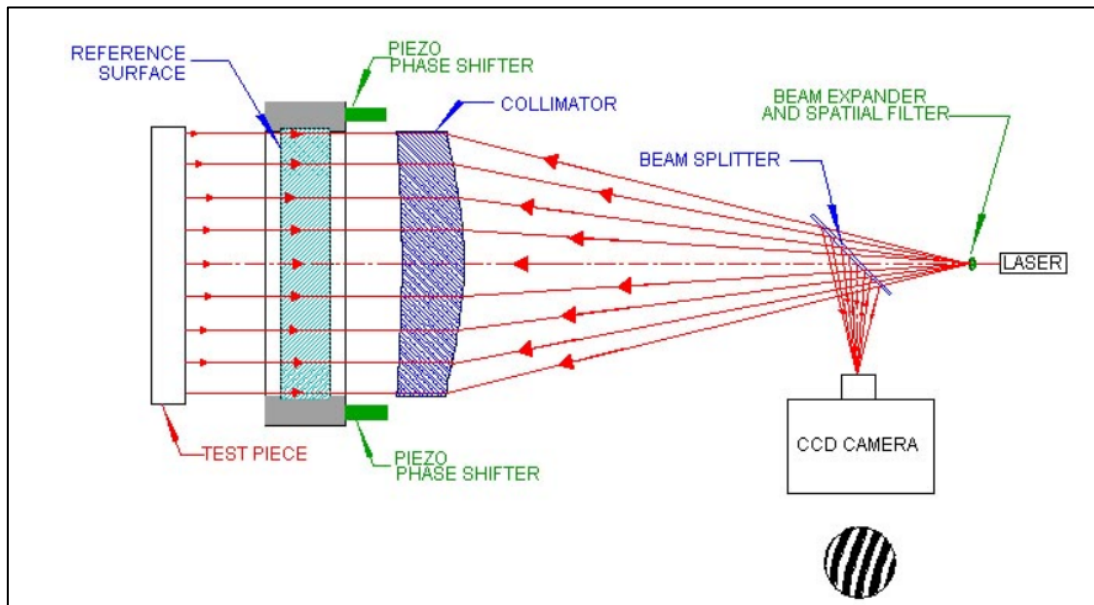
Figure 19. The interferometry process is illustrated.

Light from the laser beam passes through an expander and into the beam splitter, where some of the rays pass to the ccd camera and some of the rays move on towards the collimator. The collimator bends the beams to become parallel, and then the beams pass through a piezo phase shifter and then through a reference surface. The beams then reflect off the test piece and return through the reference surface, piezo phase shifter, and collimator. The beams reflect off the beam splitter and are focused into the ccd camera. Since the beams that reflected off the test sample have gone through a phase shift and traveled a different distance, they interfere with the original beams of light. Beams that travel different distances interfere in predictable ways, allowing the camera to interpret the interference pattern. Information from the camera is mapped into a three dimensional topography of the surface, from which roughness parameters were calculated.

47

### 4.4.3. **Roughness Measurement**

Once again, the samples were mounted in clay to provide a stable horizontal surface for analysis. Five samples were taken side by side every two inches for adequate sampling, and the scanned area for each measurement was approximately 1mm$^2$. Like in the microhardness experiment, roughness was measured along the length of the implant to see if the roughness was different to explain the implant failure. An example of the software statistics for one measurement is shown in Figure 20.
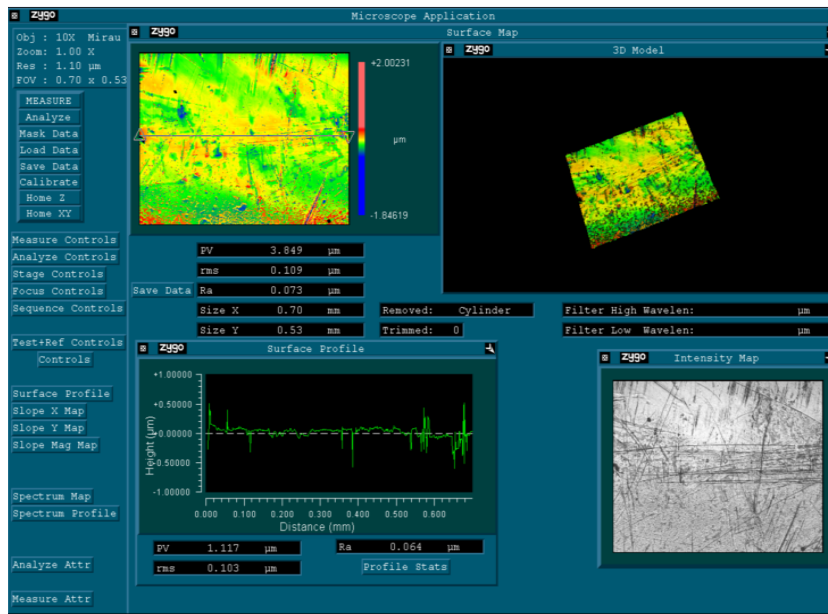


Figure 20. The Zygo surface analysis interface displays a colored topography map, a two dimensional profiler, and a three dimensional movable image.

The interface provides three images of the surface: one as seen after magnification with no alterations, one with topography by color, and one as a 3-D image

with color topography. Even though the analyzed surface area was on an approximately horizontal surface, a data transform was performed using the software to remove the slightly cylindrical tendency of the surface.

## 4.5.  Corrosivity/Passivity

Stainless steel and titanium are chosen for bone implants because of their anti-corrosive properties. However, some of the surrounding tissue images showed the dissipation of metal into the human tissue. Whether the transfer was tribological or chemical in nature remained to be determined. The passivation of the metals was tested to see if the body had an effect on the corrosive properties of the metals. Potentiodynamic polarization scanning was chosen to be the method of testing. This section describes the potentiodynamix polarization scan method, examines the test apparatus and equipment, and outlines the procedure for the test

### 4.5.1.  Potentiodynamic Polarization Scan

In a potentiodynamic polarization scan, the voltage potential is the controlled variable and the current is recorded. Contrary to standard notation, the controlled (or independent) variable is on the y-axis while the recorded (or dependent) variable is on the x-axis. There are two main regions for scanning: the anodic region and the cathodic region.

### 4.5.1.1.  **Anodic Polarization Scan**

The rest potential is the potential at which the anodic and cathodic reactions happen at the same rate, thus there is no current flow. The curve above the rest potential is the anodic polarization curve. This curve is shown in Figure 21.
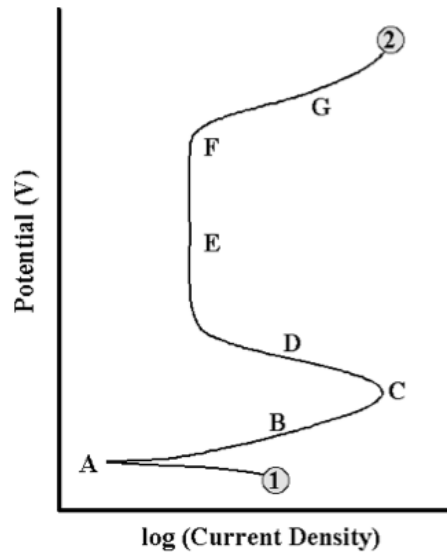


Figure 21. Theoretical anodic polarization scan of stainless steel [52].

As the potential increases from point A, the primary reaction is metal oxidation. The current density increases in region B, and this is known as the active region. Point C is the passivation potential, and the current density decreases after the potential increases past this point. The passive region (E) is notable, as the current density remains constant for a large region of voltage change. Point F is the breakaway potential, and after this point the current increases as potential increases (G).

### 4.5.1.2. Cathodic Polarization Scan

The cathodic polarization curve is under the rest potential, and the theoretical curve is shown below in Figure 22.
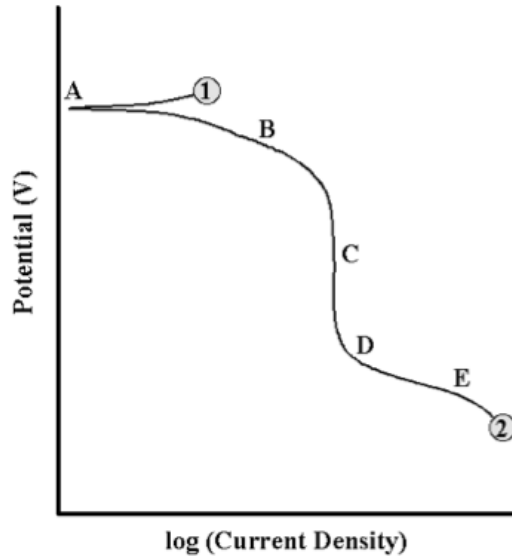


Figure 22. Theoretical cathodic polarization scan of stainless steel [52].

In the cathodic region, potential is generally varied from high to low. Point B represents the oxygen reduction reaction. The current density remains constant for a region (C) before another cathodic reaction takes place (D).

### 4.5.2. Gamry Reference 600 Potentiostat Machine and Equipment

To calculate the corrosion potential, potentiodynamic polarization testing was performed using a Gamry Reference 600 Potentiostat machine. A Saturated Calomel

Electrode (SCE) probe was used for a reference point. The approximate range of potential for stainless steel was determined from literature to be -1.2V to 0.4V. A solution of 2% NaCl in de-ionized water was used as the electrolyte. Figure 23 shows the test setup.
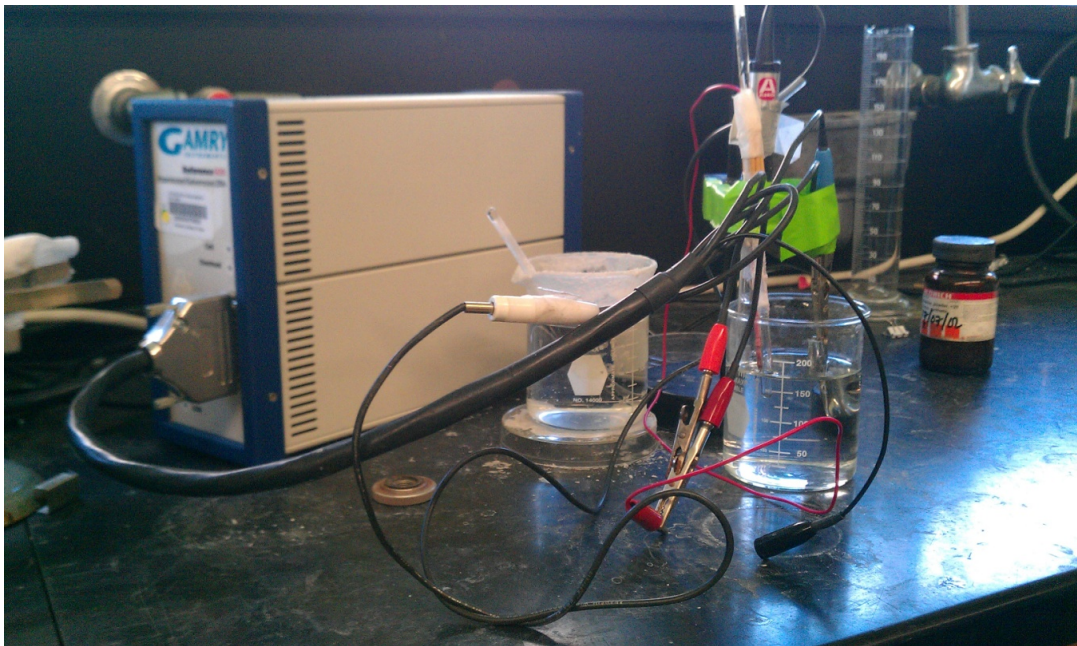


Figure 23. This figure shows the potentiodynamic polarization setup
with the Gamry Reference 600 Potentiostat

### 4.5.3. **Procedure**

For the samples, a one-inch portion was sawed off of the intramedullary nails. Tape was used to section off a specific area for testing. The exposed area was then measured in $cm^2$. The test ran for approximately three minutes to span across the voltage

range. The Gamry instrument measured the current across the voltage range, and corresponding software was used to record the data.

## 4.6. Scratch Testing

The scratch testing comparison was performed to further characterize the surface mechanical properties of the samples. Previous microhardness testing had revealed strange fracture patterns and cracks at the fringe of the indentations, and scratch testing would amplify the effects of deformation and fracture at the peripheral of the marking. This behavior would give insight into a possible surface coating removal or formation in the human body. The data extracted in this test would only be meaningful in comparison, and would not be useful for reference of standards.

### 4.6.1. Procedure

A CSM Instruments tribometer was used to create a scratch using a drill bit as the hanging mass. Figure 24 shows the tribometer test setup.

Figure 24. The tribometer doubled as a scratch tester when a drill bit
was used in place of a ball bearing.

The tribotester setup contains a sitting mass and a hanging mass, designed to remove all force from the point of contact except for the intended mass added above the test sample. The hanging masses can be seen as two circular weights on the leftmost side of the picture. The hanging mass includes everything above the sample except the disc, which was the intentionally added mass. A circular motion mechanism was converted into a linear motion to form the scratch. The black machine contains the motion mechanisms.

Each of the scratches was performed along a horizontal axial ridge of the sample, and ranged from 0.5 to 1 inch. The angle of the drill bit was 120 degrees and the force applied to the drill bit was 3N. The tribometer arm had to be manually raised after one linear movement, since the minimum movement was one cycle back and forth.

### 4.6.2. **Data Interpretation**

The scratch width and depth were analyzed using the Zygo instrument and software. Figure 25 provides a picture of the software analysis of a scratch.
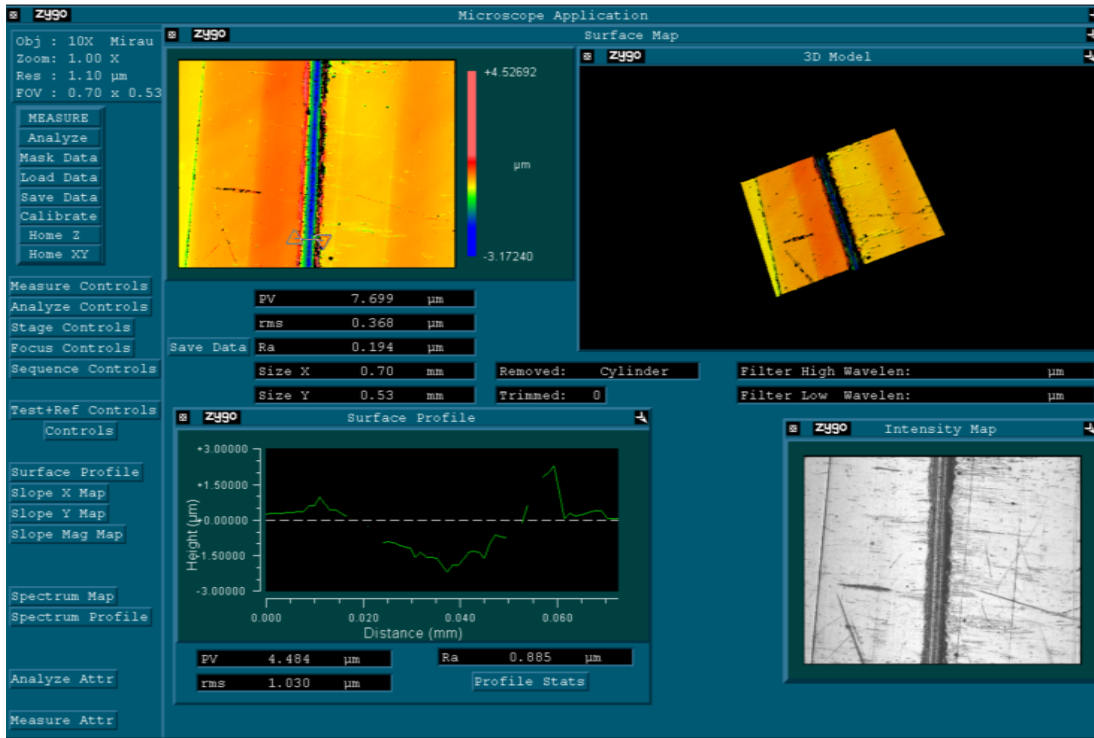


Figure 25. The Zygo interface during surface analysis of a scratch
created with the tribometer.

As seen in the figure above, a profile of the scratch is formed by dragging two reference points to create a line perpendicular to the scratch in the topographical map. A 2-D profile was generated, as seen in the figure above. Figure 9 shows another profile and the metrics used to measure the width and depth.
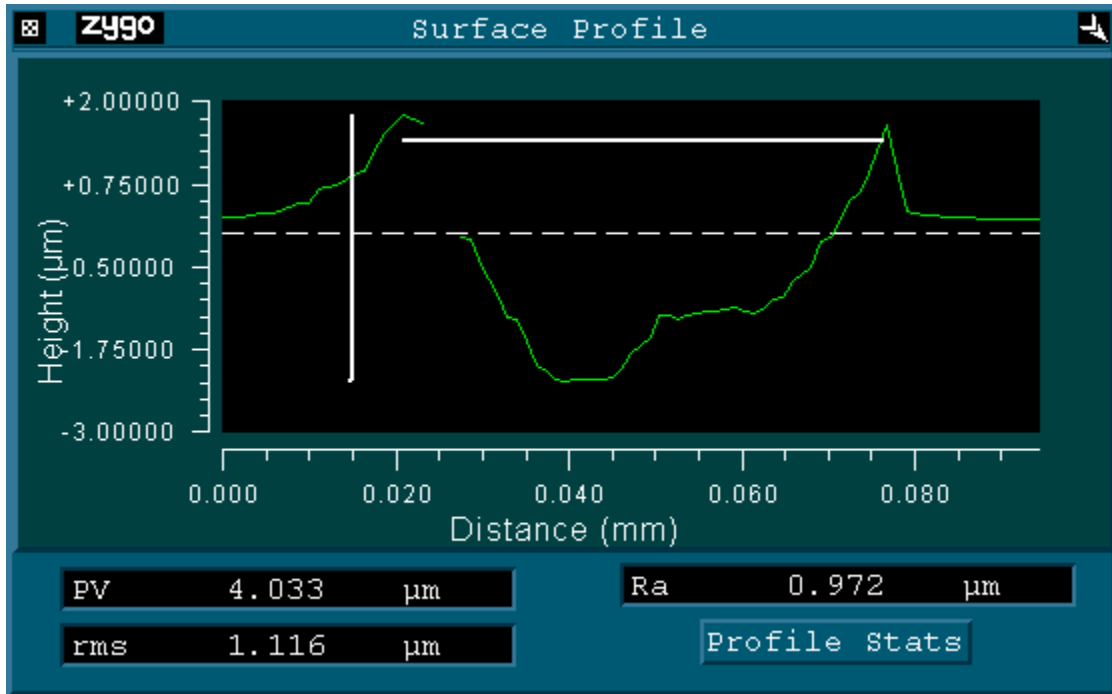
Figure 26. Two dimensional profile from the Zygo surface analysis
software interface.

As seen in the figure above, the height is defined as the distance from the highest point to the lowest point of the profile. The width is defined as the distance between the local maxima on either side of the ridge. For each scratch, five profiles were recorded. An optical microscope was used to image the surface to analyze the material pile-up at the peripheral of the scratch. Images were recorded for comparison from each of the scratches.

## 4.7. Microstructural Analysis

After the samples had been mechanically tested, they were examined at the microstructure level. The first set of experiments investigated the mechanical

degradation at the surface by testing mechanical properties, but the results could never identify a cause. This second set of experiments explores the properties of the materials that could shed a light on the degradation mechanism.

### 4.7.1. Microstructural Analysis Sample Preparation

This portion of experimentation needed to be performed after the mechanical tests because sections of the implants needed to be cut off and embedded in an epoxy plug. The following sections detail the methods for polishing and etching the samples.

#### 4.7.1.1. Polishing

The samples first needed to be cut with a power hacksaw to remove a 0.5 inch long piece. These samples were embedded into an epoxy mount using the machine shown in Figure 27.

Figure 27. The Simplimet mounting press machine comes equipped
with a pressure gauge, a heating cylinder, and cooling fins.

The sample was placed in the compression cylinder and ten grams of Buehler red

Phenocure powder were poured on top. A hollow heating cylinder was placed over the

compression cylinder to melt the epoxy. The compression chamber was pressurized to

42 ksi for fifteen minutes. The pressure was then released and the heating cylinder

turned off and removed.

Next, a polishing machine was used to reveal a smooth surface for etching. An

Ecomet 3 polishing table was used in conjunction with an Automet 2 polishing head;

both are shown in Figure 28.



Figure 28. The Automet 2 polishing head mounts on the Ecomet 3
polishing table. Each machine is equipped with controls that are
integrated with the other.

The machine was equipped with controls for time, head rpm, head spin direction,

applied force, and base rpm. The sample mount was designed to carry six samples, and

Figure 29 shows the machine with the sample mount.

Figure 29. The samples were placed in a fixture, which attached to the
rotating polishing head.

After a consultation with Buehler, the manufacturer, a procedure for polishing

the 316L was solidified. The polishing would be done in four steps, and Table 9

summarizes the test conditions.

Table 9. Test conditions for polishing stainless steel 316l samples.

| Condition | Step 1 | Step 2 | Step 3 | Step 4 |
|---|---|---|---|---|
| Central Force | 21 lbs | 21 lbs | 21 lbs | 21 lbs |
| Head Speed | 60 rpm cw | 60 rpm ccw | 60 rpm ccw | 60 rpm ccw |
| Base Speed | 250 rpm ccw | 150 rpm ccw | 150 rpm ccw | 120 rpm ccw |
| Time | 4 minutes | 4 minutes | 4 minutes | 4 minutes |
| Polish Pad | Si Carbide 320 | Ultra Cloth | Trident Cloth | Micro Cloth |
| Polishing Solution | Water | 9 um diamond suspension | 3 um diamond suspension | Collodial Silica (30%) |

Between each step, the sample was rinsed with de-ionized water and wiped dry with a Kim-tech wipe. If a chemical film formed on the surface from the solution, then sometimes acetone or ethanol were used to clean the surface.

### 4.7.1.2. **Electro-etching**

After the surface was polished to the point of no visible scratches, the samples were etched electrochemically to reveal the microstructure. The Aqua Regia solution was used as the electrolyte. Aqua Regia contains three parts hydrochloric acid to one part nitric acid. The solution was often diluted with water for some of the tests, but this only affects the amount of time for which the sample should be etched. The test sample, which served as the anode, was attached to the positive terminal by a copper wire, and the negative terminal was attached to a graphite rod, which served as the cathode. The voltage used was six volts, and the time immersed in the solution was five seconds.

Since the electrolyte was an etching reagent even without the electric current, the voltage was applied and the time elapsed when the anode was dipped into the solution. The anode (or the test sample) was not allowed to remain in the Aqua Regia solution even without the current, as non-uniform etching and pitting would occur. Quickly after the anode was removed, it was rinsed with de-ionized water and dried with a Kim-tech wipe.

**CHAPTER V**

**EFFECTS OF HUMAN BONES ON SURFACE PROPERTIES OF IMPLANTS**

This chapter discusses the effects of the human body on the morphology of the implants and the corrosion behavior after implantation. The chemical and microstructure of implants were studied using electrochemical potentiostat and optical microscopes.

**5.1. Corrosive Behavior**

The potentiodynamic study reveals corrosive behavior of samples before and after implantation that reflects the surface properties of the same. The results of the potentiodynamic polarization scans are posted in Figure 30 and Figure 31.
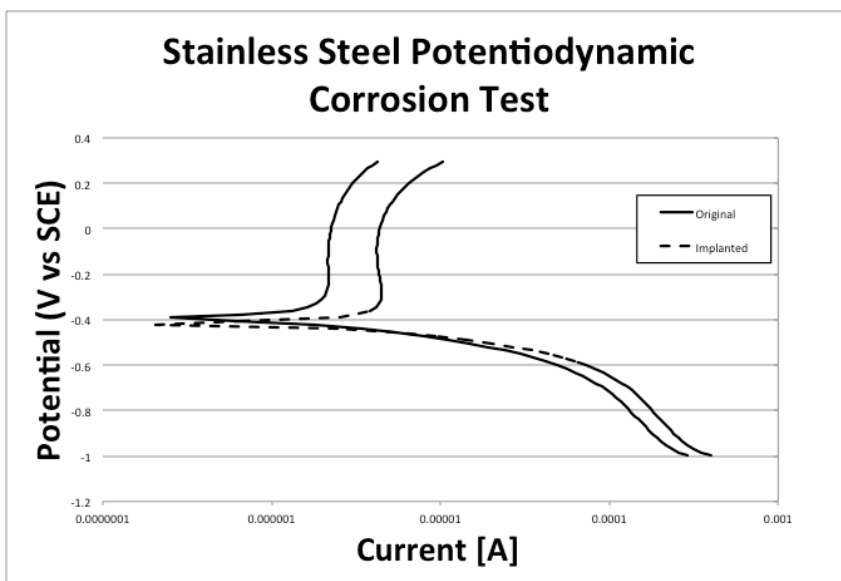


Figure 30. Potentiodynamic polarization curves for stainless steel long femoral intramedullary nails.

The most telling sign of this result is that the passive region for the implanted material occurs at a much higher current than for the non-implanted material. This implies an increased chance for corrosion for the implanted material if the two materials were placed in the same environment. The difference morphologically could possibly be explained by the removal of a surface treatment used for all implants, or also by the deposition of an oxide layer that changed the corrosive properties of the steel. Results shown in Figure 30 indicates that the reference sample gets passivated earlier that the implanted one. This has several possible reasons. The first is the surface roughness effect that the rougher surface is prone to be corroded more because it traps more liquid inside the valleys. The second reason is the surface chemistry of both samples. If a protective layer preexists, the passivation can only make it better as shown in the steel case. The encapusulation and biological attack on the implant surface is possible we will look into this later in this chapter. Ultimately, the implanted sample surface is rougher than the reference sample. This will be shown in the following section.
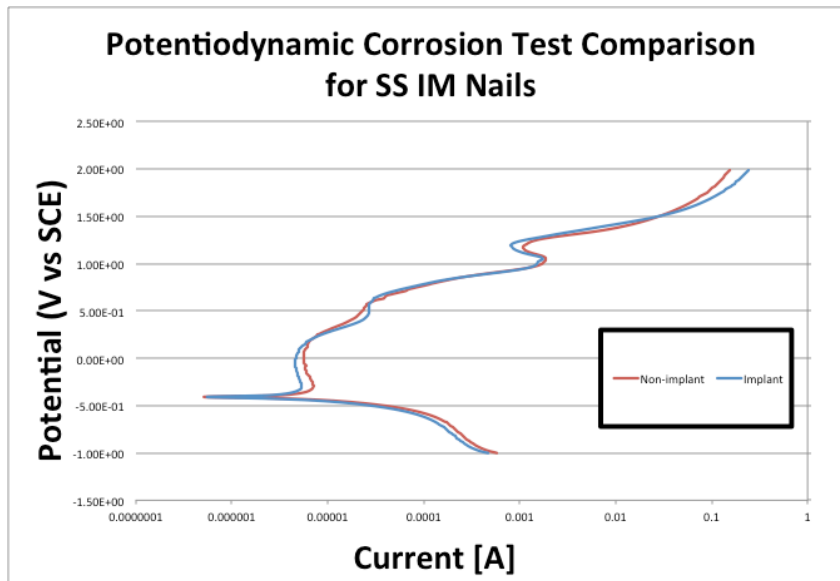
Figure 31. Potentiodynamic polarization curves for stainless steel tibial
intramedullary nails.

The potentiodynamic polarization scan for the tibial nails was less conclusive
than the previous evidence. There are slight deviations between the curves, but the
differences are negligible and no claims can be made regarding the changes in
passivation for the material. Higher potential range along the anodic scan were shown in
this graph and still no significant differences appeared. No significant differences occur
between the rest potentials, the passive regions. The difference between this implant and
the previous one was that this was a tibia implant while the other was a femur implant.
The fact that the tibia naturally experiences less stress than the femur (due to sharing
load with the fibula) may have bearing on the lack of evidence for property alterations.

## 5.2. Surface Roughness / Corrosion Sites

The surface roughness differences were apparent throughout all the stages of experimentation in the stainless steel samples. Some of the differences could be seen with the naked eye, and are quantified in the following chapter. The titanium bore significant signs of scratching and wear, although the locations and severity of the damage hinted that the damage occurred during removal from the bone. Both implanted and non-implanted materials experienced a mild degree of scratching or rubbing from shipping and handling. The implanted material also bore pits, explainable by corrosion. Images of the surface damage from the long femoral nails are shown side by side in Figure 32.
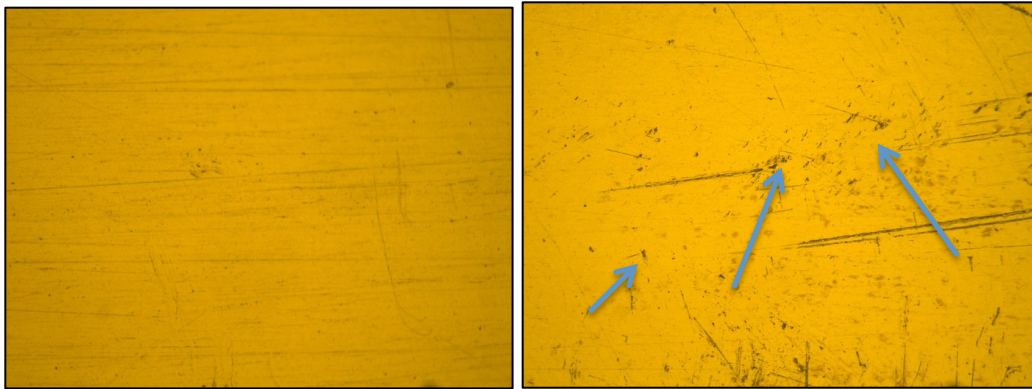


Figure 32. A typical view of the surfaces is shown for the stainless steel long femoral intramedullary nails, non-implanted (left) and implanted (right). Arrows indicate pitting.

As seen in the images, deeper scratching has occurred in the implanted material; this is intuitive as the material was scratched and rubbed by the bone during fixation and

possibly over time in the body. Localized pitting also appears in the implanted sample, indicating that a chemical reaction has occurred. Given that stainless steel is known to corrode in fixation applications, this is likely.

## 5.3. Scratch Deformation Analysis

An optical analysis was used to evaluate the scratch deformation patterns in the tested materials. Significant plowing occurred in all cases, and the material build up is easily visualized from the profile shown in Figure 33.
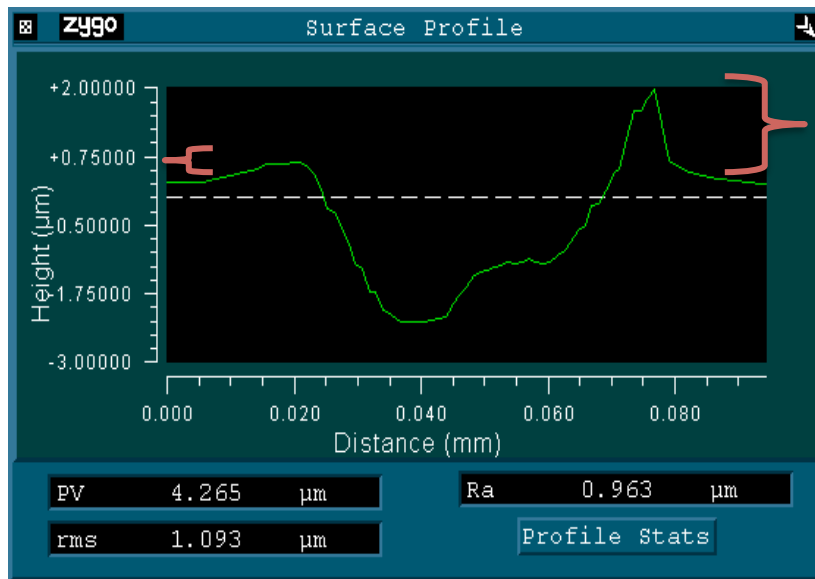


Figure 33. The profile of the scratch from the Zygo surface roughness
analysis interface for a stainless steel long femoral intramedullary nail.
Brackets indicate pileup height.

The material is pushed to the side during abrasive wear and builds up at the edges of the valley. Optical images of the scratches were taken to characterize the deformation

as brittle or ductile. The fracture pattern of the material speaks about dislocation pile-up in the microstructure. Images of scratches are shown in Figure 34 and Figure 35.
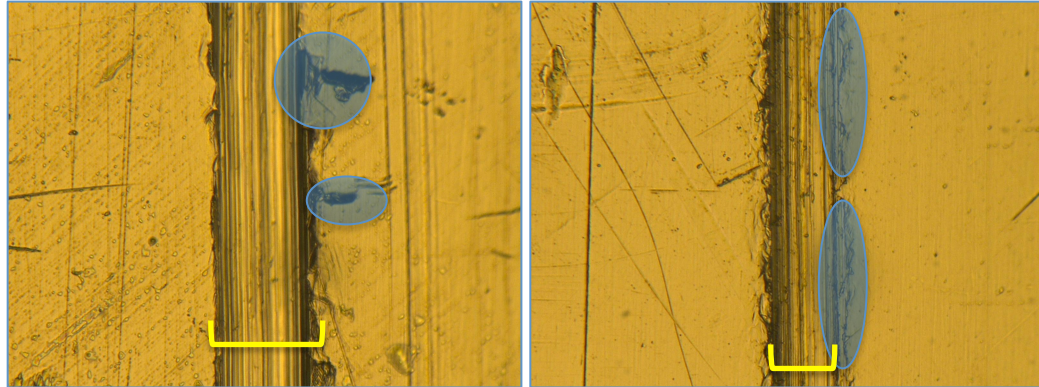


Figure 34. The images from the scratch tests are compared for the stainless steel long femoral intramedullary nail case, non-implanted (left) and implanted (right).

Brittle material exposed to plowing is characterized by cracks to the outside of the buildup material. The figures show that both of the materials contain cracks, but the implanted material contains more cracks. Blue circles highlight the buildup formation, and evidence of adhesive wear is shown in the non-implanted sample. This is evidence of ductility, whereas more frequent smaller and uniform cracking indicates brittleness. Another factor to consider is that the scratch is thinner (marked by brackets) – and thus shallower by geometry – and so less material has been displaced. The surface of the implanted sample is generally more resistant to scratch deformation. The implanted material appears to be more brittle than the non-implanted material.
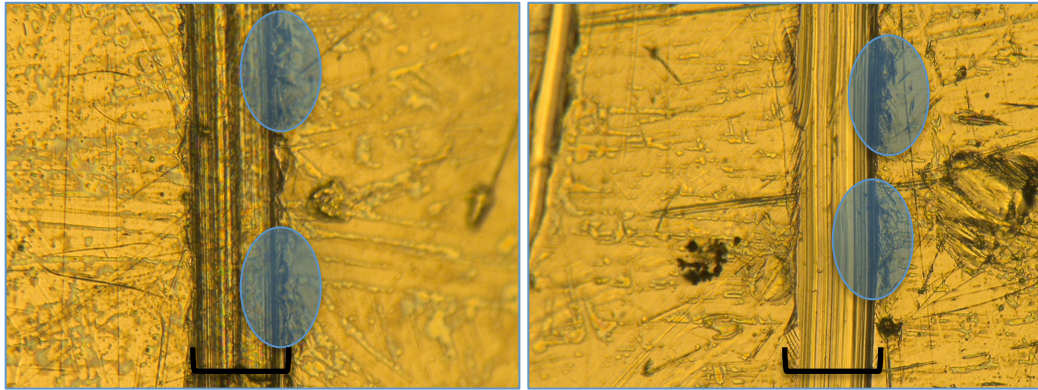
Figure 35. The images from the scratch tests are compared for the
stainless steel tibial intramedullary nail case, non-implanted (left) and
implanted (right).

In the case of the tibial nails, the difference is less apparent. The width is almost
identical (shown with brackets), and the deformation pattern is similar. Blue circles on
the figure mark areas of cracking but one material does not seem to be significantly more
brittle than the other. This coincides with the lack of evidence for difference in the
potentiodynamic polarization scan. Again, the evidence does not show that the tibial
implant has experienced significant change.

## 5.4. Microstructural Analysis

The samples were etched so the microstructure could be analyzed. Both
brightfield and DIC images of the samples appear in this section. The microstructure was
analyzed to identify the mechanism for the changes documented earlier in this chapter.
Microstructure images for all of the stainless steel samples appear in Figure 36, Figure
37, Figure 38, and Figure 39.
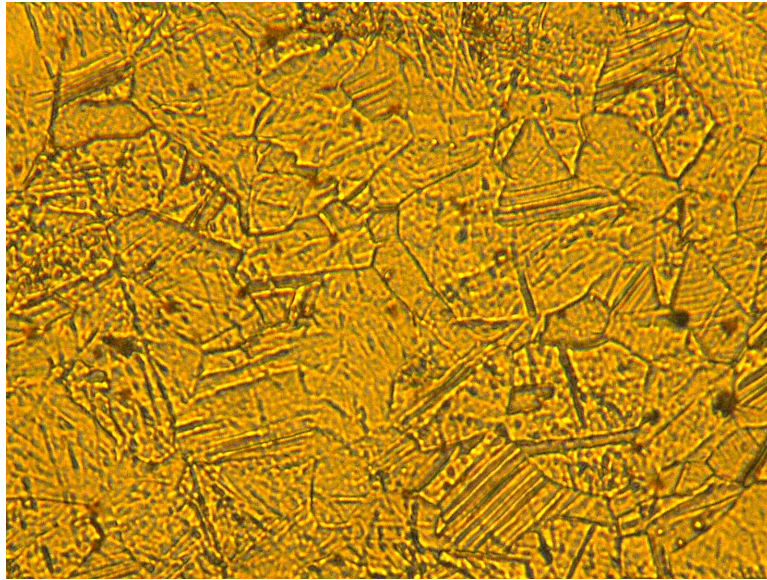
Figure 36. Microstructure of the non-implanted stainless steel long
femoral nail (2000X magnification).

The grain boundaries are well defined in this image, and the austenite phase is
clear. The micrograph shows partly recrystallized austenite grains. Remnants of
twinning remain. The matrix is austenite [53].
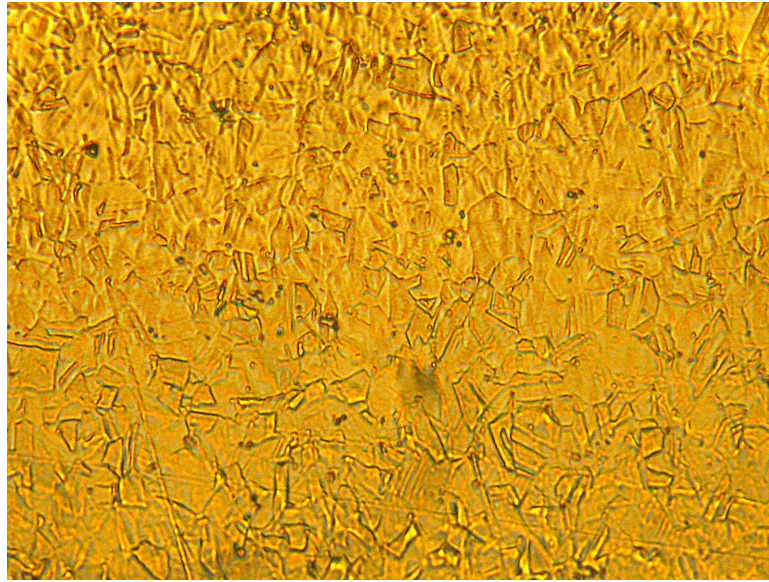
Figure 37. Microstructure of the implanted stainless steel long femoral
nail (2000X magnification).

Here the grain boundaries are fainter and selective etching has occurred. The underlying material has been etched unlike in the non-implanted sample – presumably due to a chemical alteration of the material due to corrosion. The material was made susceptible to corrosion by the damaging and removal of the chrome-rich oxide layer, leaving a chromium depleted surface [54]. In the absence of chromium, portions of the underlying metal have been etched away [53]. The selective etching appears to have occurred in a pattern that would suggest that the implanted material has a smaller effective grain size. This would only hold true for the effected surface layer, but still bears weight on the properties of the material.
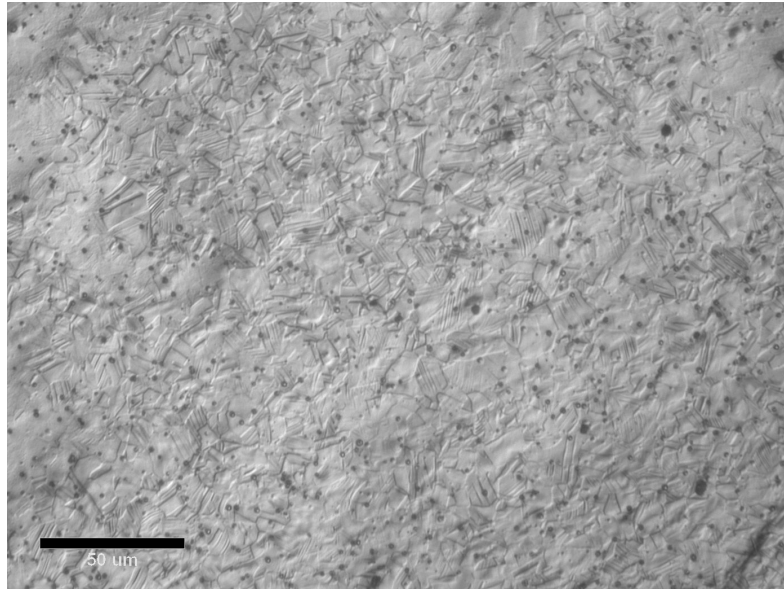
Figure 38. DIC image of the microstructure of the non-implanted
stainless steel tibial nail (20X, 0.5 NA objective).

The etching shows distinct grain boundaries, but the contrast from the differential

interference contrast image shows that the etched surface is not completely flat. The

tibial implants have not shown significant change thus far, so let us examine the

implanted sample to see if any noticeable differences have occurred.
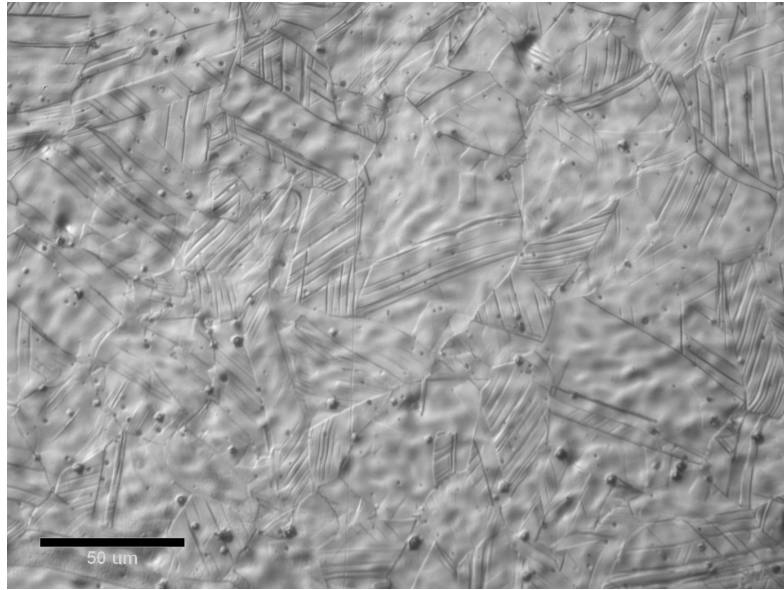
Figure 39. DIC image of the microstructure of the implanted stainless
steel tibial nail (20X, 0.5 NA objective).

The difference in microstructure is not apparent after observing the implanted

sample. The grain size appears to be larger but there is no reason to think that the grain

size changed, rather that the direction of the grains might be different. The topography

shows that both surfaces etched similarly, and the same effects from the femoral samples

are not apparent in the tibial samples.

**CHAPTER VI**

**ALTERATION IN MECHANICAL PROPERTIES OF IMPLANTS**

This chapter discusses about the mechanical properties of the implants that the human body has changed. The interpretation of the surface morphology analysis leads to the idea of macro-scale changes in the material. The properties measured in the previous experiments of Chapter III are extrinsic, and are merely indicators of a change in intrinsic properties.

This section discusses effects of human body on mechanical properties. Results showed both a change in hardness and wear resistance of the implanted surface. The interpretation of the microstructure analysis helped to explain the change in mechanical properties.

**6.1. Effects of Human Body on Hardness of Implants**

As was seen in the microstructural analysis, the human body has certainly affected the change in properties of the bone fixation materials. In this section, the results form the mechanical tests are presented to show the changes that the human body had on the hardness.

6.1.1. **Hardness**

The hardness results are shown in Figure 40, Figure 41, and Figure 42. Figure 40 has two plots of data. The top one is for samples that have been implanted inside the human femur, and the bottom plot is for the control sample that was not implanted. In comparing two plots, the difference is that the implanted samples are significantly

harder, and that is consistent throughout the measurement. Through repeated

experiments, results shown evidence that the surface of the implanted material had

become higher than that of the non-implanted material in the case of the long femoral

nails. An image of the tested implants appears beneath each set of data to match the data

to the samples.



Figure 40. The hardness data for the long femoral nails shows that the
surface of the implanted sample was harder on average.

The hardness data shows that the implanted long femoral nail was harder than the

non-implanted long femoral nail. None of the error bars came within 10% of each other,

so this is stated with certainty. The implanted sample had a peak in hardness in the bent

75

area, presumable due to dislocation pileup that occurred at the deformation. Both samples also showed that the hardness was higher at inches 1 and 2, explained by the presence of screw holes that imply cold working as a result of manufacturing technique. It is interesting to see that the shape of the plots correspond with the shape of samples. The shape of the data points almost changes exactly to match the shape of the deformed implant. This might indicate that the mechanical properties of their bulk follow the same trend of the surface. This will be further discussed correlating with stress distribution discussed in Chapter III.





Figure 4.30. The hardness data for the hip orthopedic oral nails show what the surface of the implanted sample was hardened the fracture points.

The hardness values were close in most cases, and a significant difference between the samples was not apparent. In the implanted sample at the fracture point, the average hardness was higher than the rest of the values for both samples. These measurements were taken on a different axial ridge due to the screw holes, so this may have caused discrepancy in the data at that point.
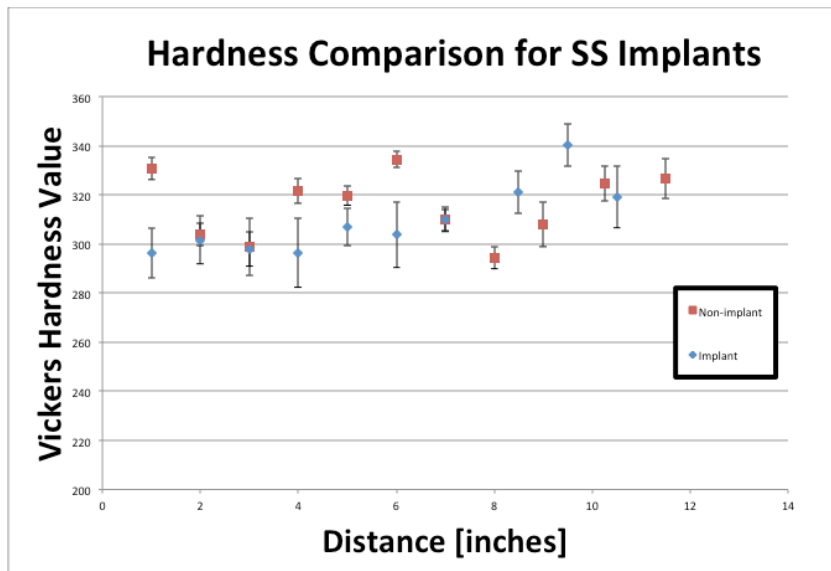


Figure 42. The hardness data for the tibial nails is inconclusive in interpreting a significant difference.

The hardness data for the tibial nails was erratic and inconclusive. The hardness data along the length varied dramatically for both samples, and switch between one implant being harder than the other. No significant difference could be concluded from the data.

While the tibial nails were not able to offer a conclusion, the long femoral nails present intriguing data for the whole length of the sample regarding a change in hardness. The data from the short femoral nails showed evidence of increased hardness around the fracture location. The inconclusive samples might be due to the following reason, implanting time, the activities of the patient and the age and gender. Since the source of our samples is limited, we will continue investigator on those factors in future. In the present research, we will focus on the evidence for the current samples.

Table 10. This table compares the Brinell hardness values for the
titanium femoral plates.

| Sample | Hardness | Standard Deviation |
|---|---|---|
| Non-implanted | 81.77 | .058 |
| Implanted | 77.87 | .961 |
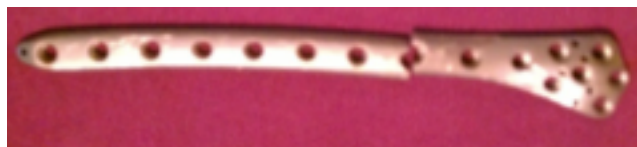
The hardness values for titanium show approximately a 5% increase between the non-implanted and the implanted samples. This difference is small compared to the difference shown in the steel femoral samples. The data is presented differently due to a different hardness test being performed, as explained in the experimental section. From this hardness data, we can say that the hardness of the titanium was not significantly altered.

### 6.1.2. **Evaluation of Surface Roughness**

Figures Figure 43, Figure 44, Figure 45, and Figure 46 are roughness average of the samples. Each of these figures shows both the roughness average data and the image of the samples to correspond to the data. The roughness average results were interesting and they showed that the stainless steel implanted samples were significantly rougher. Every one of the roughness tests for the stainless steel demonstrated that the implanted samples were rougher, even though some of the tests only proved this for the failure site. The relationship between roughness and hardness reflects the surface property – performance of a material. For a ductile material, roughness average bears an important correlation to surface hardness, as the deformations in the material lead to surface dislocations that pile up to increase surface stress and hardness. Although these dislocations due to roughness exist primarily at the surface, these stress intensification factors can compound to lead to complicated failures in the material. Another possibility is that the increase in hardness also correlates to a more brittle material – susceptible to crack propagation. In addition, if there are any chemical reactions between the implant

and surrounding tissue resulting in corrosion, the surface roughness of the implant could be increased. To confirm which factor(s) dominate, further analysis is carried out that are discussed in the following sections.
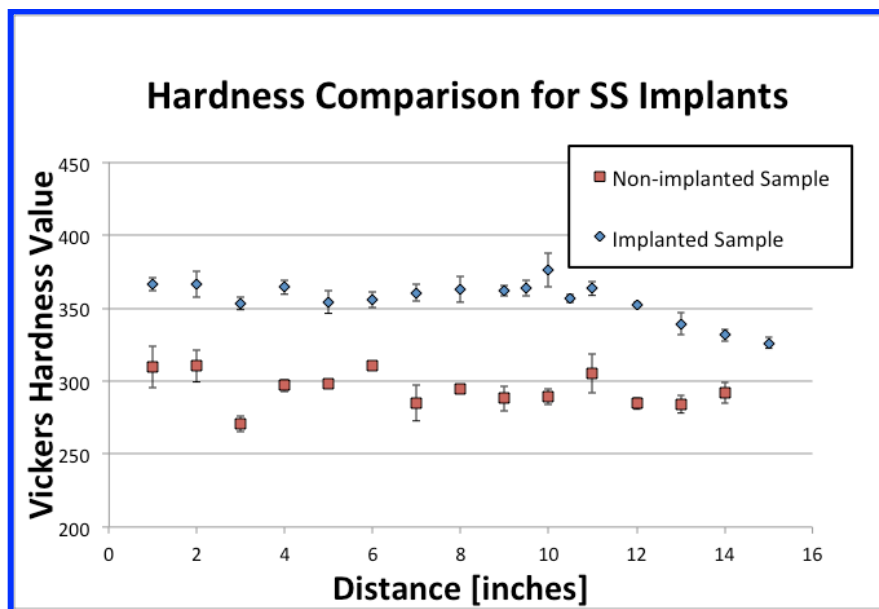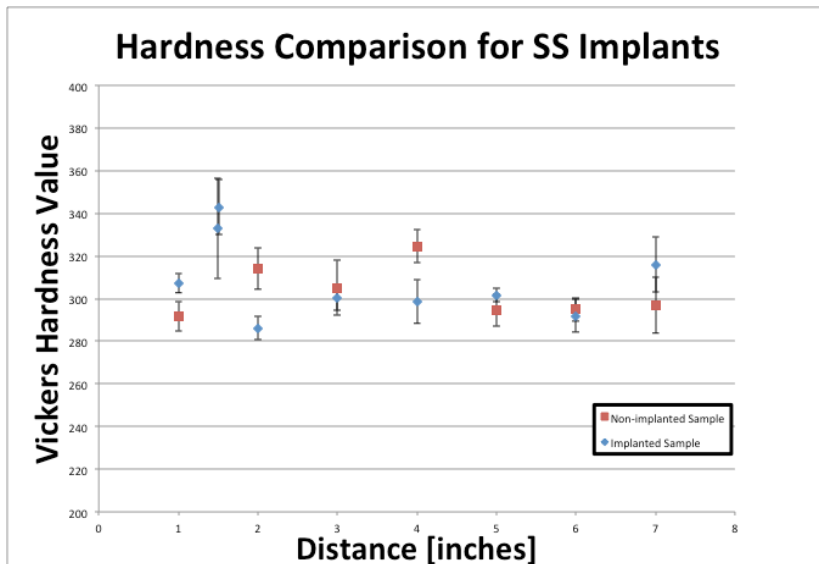


Figure 43. The roughness average data for the long femoral nails shows
that the surface of the implanted sample was rougher on average.

The roughness average data shows that the implanted long femoral nail was significantly rougher than the non-implanted long femoral nail. The extra sampling for the implanted nail around the failure point showed an even higher roughness average

than the rest of the sample. Independent of the roughness average values, the standard

deviation was higher in the implanted sample.
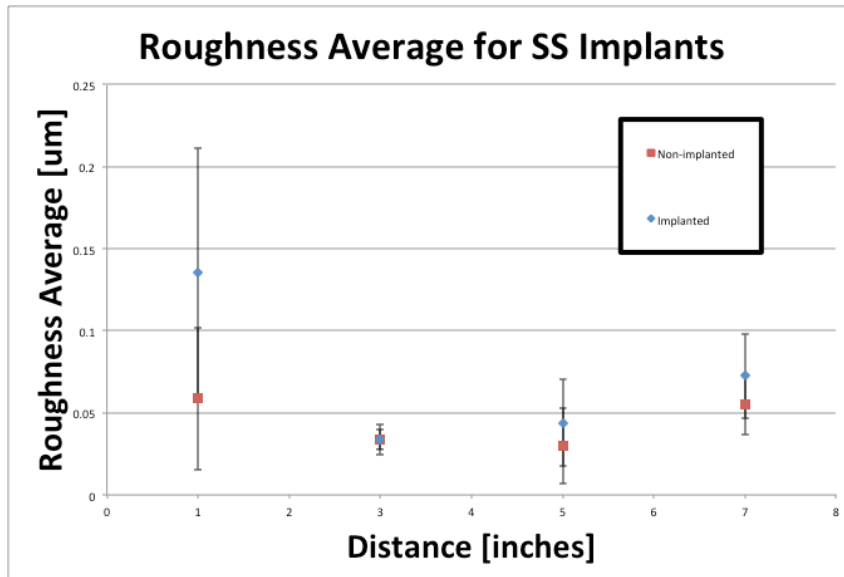


Figure 44. The roughness average data for the short femoral nails
shows no conclusive evidence for a difference, but it appears that the
implanted sample is rougher on average.

The error bars for the stainless steel short femoral nails overlap at every point

that measurements were taken. This fact makes it difficult to conclude with certainty that

The implanted sample is rougher, although the averages are higher at every measured

point. On its own this data might present a weak case, but the findings strengthen a

compelling argument with a repeatable trend: that is, that the implanted samples are
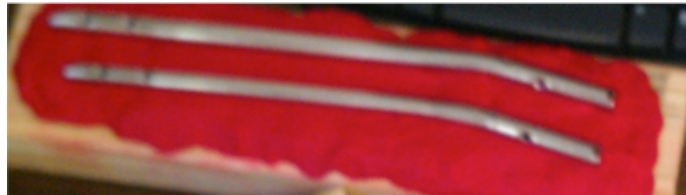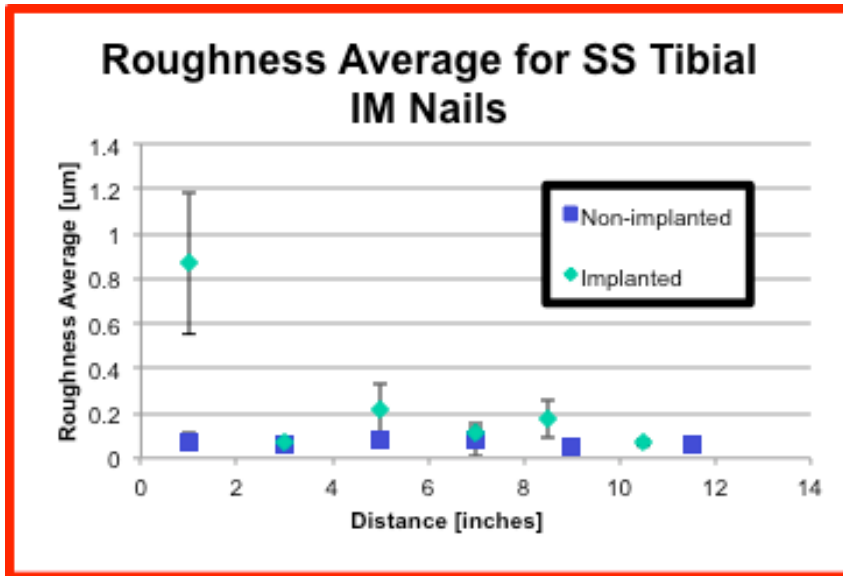
rougher.



Figure 45. The roughness average data for the tibial nails shows that the
surface of the implanted sample was rougher on average.

The roughness measurements for the stainless steel tibial implants show that the

roughness average is higher for the implanted sample than for the non-implanted sample.

The measurements for inch 1 of the implanted sample display a roughness average much

higher than the rest of the measurements. This is related to the fracture at the screw hole,

around which the surface is rough even to the naked eye. The standard deviation for the

implanted sample's measurements was noticeably higher than the standard deviation for the non-implanted sample's measurements. At all points, the average of the data measurements was higher for the implanted sample than for the non-implanted sample, and for half of these locations the error bars did not intersect.
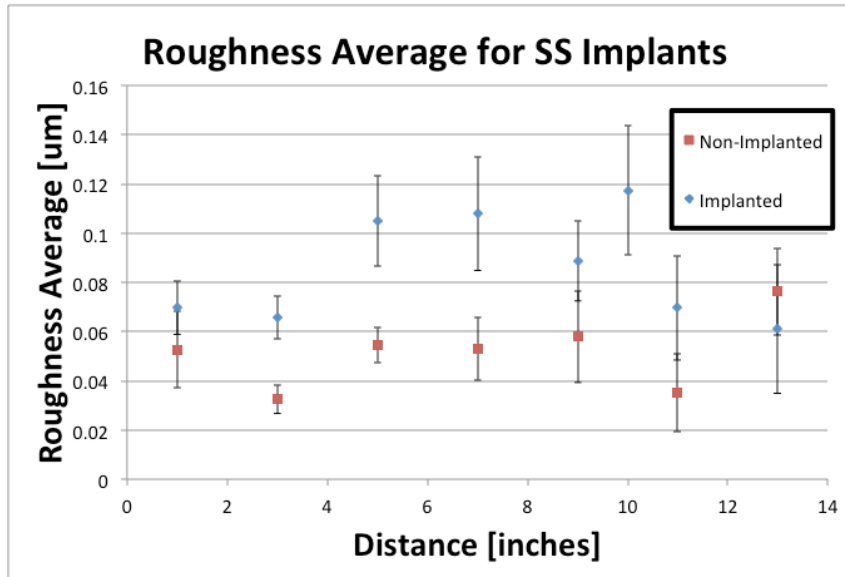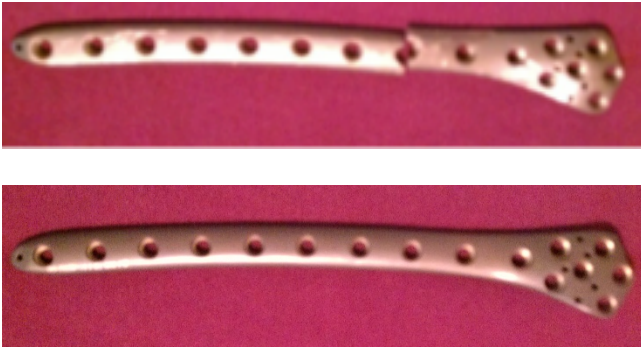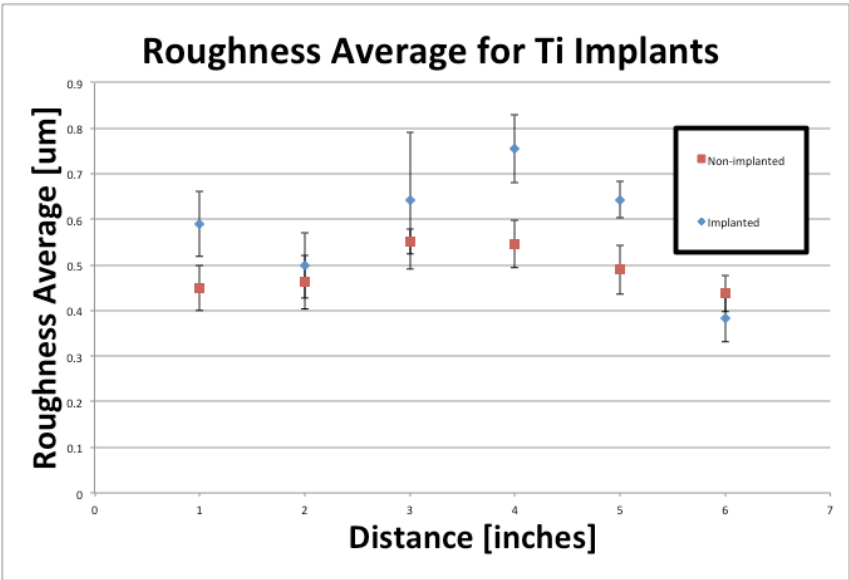


Figure 46. The roughness average data for the femoral plates shows that the surface of the implanted sample was rougher on average.

The roughness data for the titanium femoral plates is inconclusive in that there is no significant difference in roughness between the implanted and non-implanted sample. Many of the error bars overlap, and the averages are close in value.

All of the stainless steel roughness average evaluation tests support that the surfaces of the implanted samples are rougher than the surfaces of the non-implanted samples. The titanium roughness average evaluation concludes that there is no significant difference between implanted and non-implanted sample. For the steel, the change in surface mechanical properties compounded the probability of implant fracture by introducing stress concentrations and crack growth sites.

## 6.2. Effects of Human Body on Wear Resistance

It has been well accepted that the wear resistance is a function of hardness, as shown by Archard's equation [55].

The higher the hardness of a material, the lower it wears. In the present research, wear resistance provides more conclusive evidence for the removal or displacement of material instead of just the ability to resist deformation. This provides more insight into mechanical and surface properties of the material than hardness testing would provide.

### 6.2.1. Scratch Resistance

An optical analysis of Figure 34 shown in Chapter 4 shows that the brittleness and apparently the hardness of the stainless steel femoral sample were increased after implanting into human body. The scratch tests shown in Figure 47 and Figure 48 confirmed quantitatively that the stainless steel samples have higher scratch, i.e., wear

resistance in this case - this has increased due to implantation. The physical dimensions

of the scratch were smaller than that reference material. In this sense the scratch testing

functioned as another form of a comparative hardness test. Images were also taken with

an optical microscope to characterize the material in the pileup region. This showed the

failure pattern to identify the presence of a coating or lack the lack of a coating as shown

in Chapter 4. The charts for scratch depth and width are shown in Figure 47 and Figure

48.
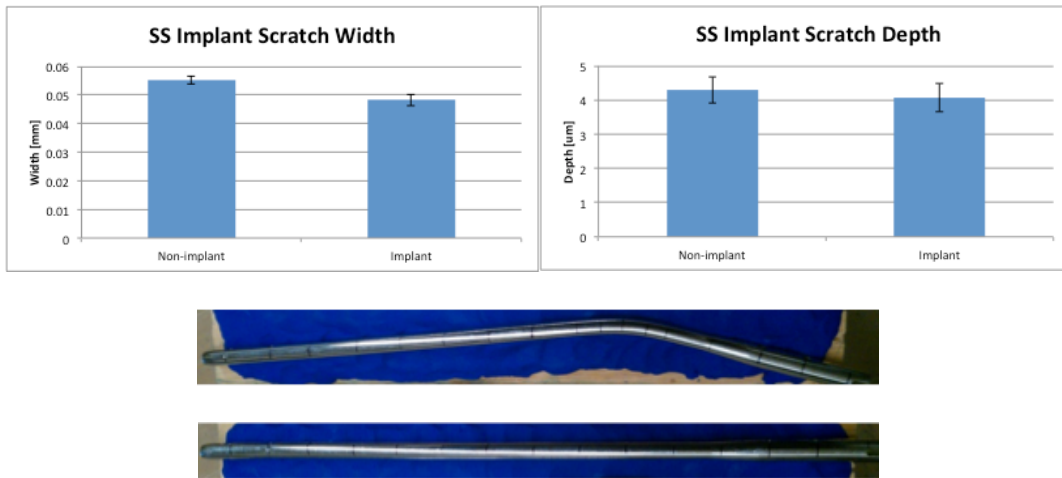


Figure 47. The scratch width and depth were smaller for the implanted
long femoral nail.

The scratch width and depth were smaller for the implanted sample. This leads to

the conclusion that the implanted materials were harder. The error bars for the scratch

width did not overlap, but the error bars for the scratch depth did overlap. A probably

cause is the deformation pattern during scratching, during which the most surface level

material permanently deformed due to hardening and the innermost material deformed plastically, recovering partially from the deformation. As the material closer to the surface was more affected, the difference in the depth is less noticeable as the depth measurement accessed the region where the two samples were likely to be similar.
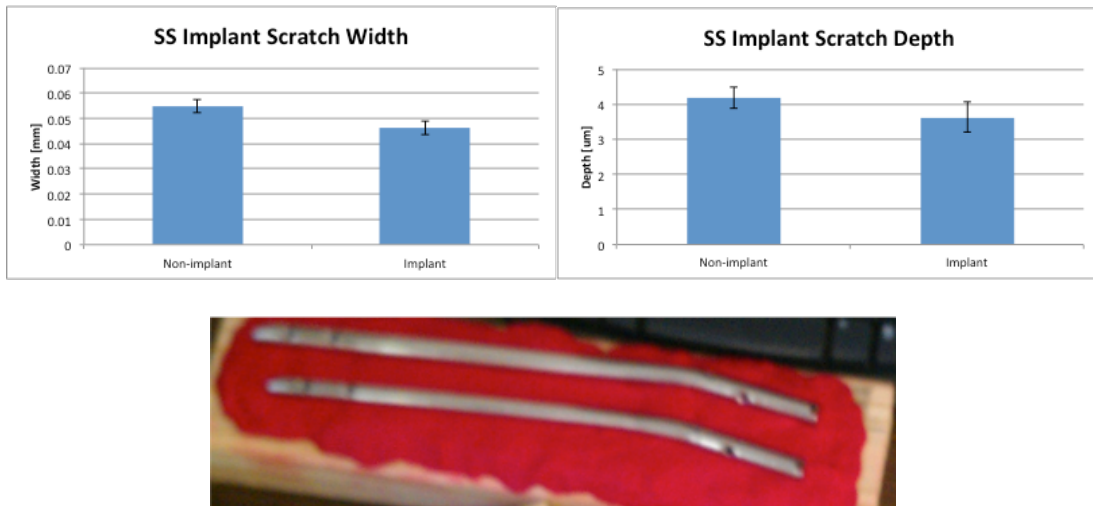


Figure 48. The scratch width and depth were smaller for the implanted tibial nail.

### 6.2.2. **Effects of Surface Roughness on Wear**

A rougher material is more susceptible to wear. This is due to the asperity contact peaks sustaining higher contact stress than the rest. The higher the surface roughness, the less number of asperity contacts, and thus the higher contact stress [56]. The dramatic change in height of the surface will cause high friction when a slider is in contact with a disk. In the present research, the wear can be seen using optical microscope and images are shown in Figure 49 and Figure 50.

Images of both the surface of the implanted material and of the proximal biological tissue are shown in Figure 50 and Figure 51. However, the material after wear occurred in the human body was still rougher than the pre-implanted material. This indicates that the wear was an effect of the roughness, not a cause. The non-implanted material was not perfectly smooth, but significantly smoother than the implanted material. An optical image of the non-implanted stainless steel long femoral nail is shown in Figure 49.



Figure 49. The non-implanted stainless steel appears to be polished although having several scratches.

The implanted material is visibly rougher, and was already confirmed by the Zygo analysis results. The roughness does not appear to be due to scratches only, but also from localized pitting, indicative of a bio-chemical attack. A similar image of the implanted material is shown in Figure 50.
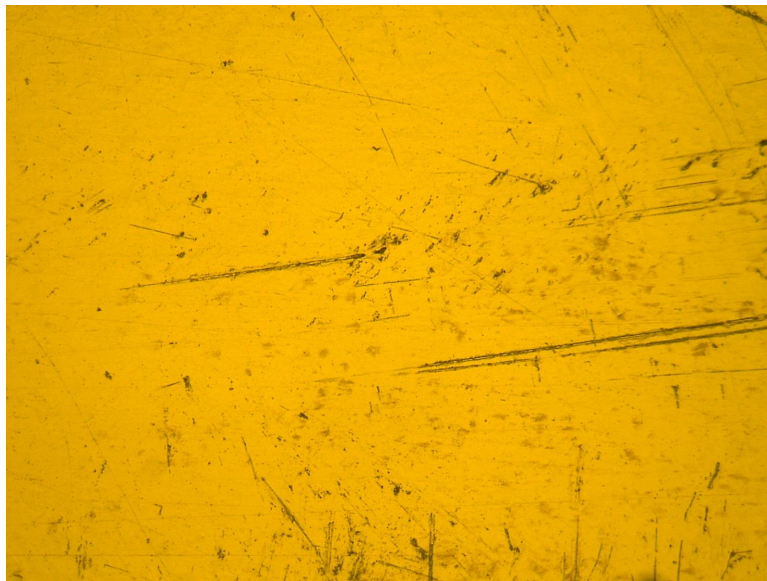
Figure 50. The implanted sample shows increased roughness due to
localized pitting.

The observed pattern of surface roughness showed a cause of deformation other than physical wear. This observance was compared with images of biological tissue proximal to the bone implant, as shown in Figure 51. The tissue sample was provided by Dr. Zhou at Shandong Provincial Hospital for Orthopedic Trauma and the image was taken by Yan Zhou at Texas A&M University. The figure shows metal fragments that lodged in the tissue. Two of these images are shown in Figure 51.
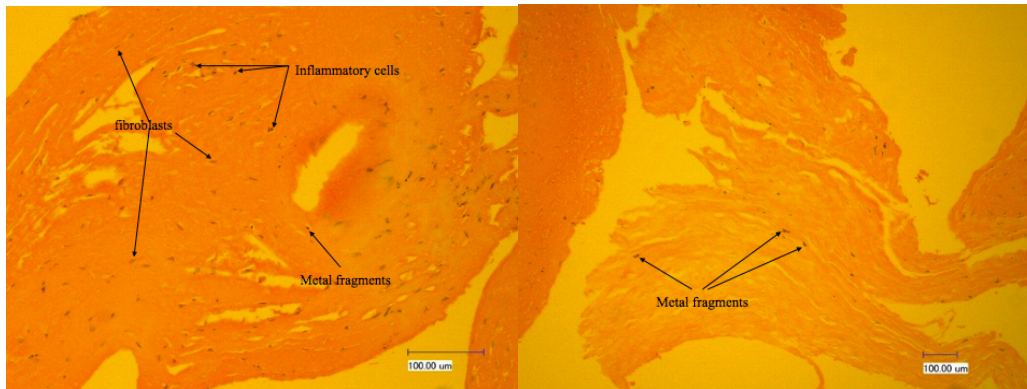
Figure 51. Tissue samples proximal to the bone implant show the
presence of metal fragments, fibroblasts, and inflammatory cells.

The tissue contains inflammatory cells – the body's response to harmful stimuli.
This indicates that metal fragments have caused the inflammation, and a few metal
fragments can be seen in the figure above. Fibroblasts also appear in the first image.
Fibroblasts are metabolically active cells in the connective tissue, and play a large role in
healing wounds [57]. The above images clearly show that material has transferred from
the implant surface to the bio-tissue, increasing the roughness and decreasing the wear
resistance.

### 6.2.3. **Microstructure Effect on Wear Resistance**

As shown from the grain size and the Halle-Pech effect, the implanted materials
certainly had higher yield strength. The smaller grains also caused an increase in
hardness, as shown in the Vickers microhardness results. The roughness proved that the
dislocation density was higher, leading to resistance of both indentation and wear. These

dislocations were caused by a biochemical reaction, and the body's response is shown in the proximal bio-tissue. The alterations to the surface do not likely confer a huge change to the bulk mechanical properties, but still lead to an increased probability of failure through stress concentration and crack propagation.

## 6.3. Chapter Summary

This chapter discussed the effects of human body on surface roughness, hardness, and wear resistance. Results showed that the hardness, roughness, and wear resistance of the stainless steel femoral implant were increased due to implantation in the human femur. The results show that the stainless steel tibial implant samples were not significantly harder, although they were rougher and more wear resistant. The titanium implants were overall unaffected by implanting in the human body. The primary reason for not conducting chemical and morphological tests on the titanium was that no mechanical properties had significantly changed.

# CHAPTER VII

# IMPLANT FAILURE ANALYSIS

This chapter discusses the failure mode, cause, and effects of the human body on implants. There are four implants studied here: Long Femoral Intramedullary Nail, Short Femoral Intramedullary Nail, Tibial Intramedullary Nail, and Femoral Plate. The failure types are identified from a macro scale analysis and mechanisms are further discussed.

## 7.1. Long Femoral Intramedullary Nail

To recapitulate on the case of the long femoral intramedullary nail, images of the implant are shown in Figure 52.



Figure 52. The x-ray and regular image show the bend in the long
femoral intramedullary nail.

The x-ray image shows a complicated fracture where the bone appears to be crushing into the right side of the intramedullary nail. This stress riser is coincident to the location of high stress shown in the simulation chapter.

### 7.1.1. Failure Analysis

The failure mode for the long femoral intramedullary nail was bending. Bending in a rod occurs due to non-axial loading and exceeding the yield strength of the material.

In light of the experimental evidence, the failure of the long intramedullary nail is an enigma. The hardness results would lead to the assumption that yield strength of the material had been changed. However, since the hardness increased while inside the human body, the yield strength would have increased with the hardness. This counters the hypothesis that the implant failed because of lowered yield strength.

This does not negate the findings in this paper. On the surface level, the hardness was higher in the implanted sample, and thus the yield strength on this surface level would have been harder. However, a bending failure would take into account the strength of the bulk material. Also, the bending failure would have happened suddenly, and changes in the mechanical properties of the surface level would not have been able to cause an impact in the bulk material like they would through crack propagation.

Thus, the mechanical properties in the long femoral intramedullary nail were certainly altered, but the altered properties were not the reason for the bending failure.

## 7.2. Short Femoral Intramedullary Nail

Although included earlier in this paper, the images of the short femoral intramedullary nail fracture are shown in Figure 53.



Figure 53. The x-ray and regular image show the bend in the short femoral intramedullary nail.

As seen in the x-ray, the bone appears to have a pre-existing mal-union that causes a stress riser at the bend. In addition, the bone fracture increases the stress in proximity to that area. As seen in the Chapter 3 on simulation, daily activity produces the highest stress on the femur shaft – right at the site of the implant fracture. The screw hole in the intramedullary nail introduces even more stress concentrations to that area.

This is why the implant fracture occurred in a slightly different location than the bone fracture. The fractography is shown in Figure 54.



Figure 54. The fractography shows a brittle fracture.

As seen in the image of the fracture, the break was brittle. The parallel cracks on middle top indicate fatigue failure. In conjunction with a decrease in mechanical properties, this fixation was a plausible candidate for failure.

### 7.2.1. Failure Analysis

The failure mode for the short femoral intramedullary nail was brittle fracture by fatigue. The fatigue occurred over a large number of cycles with stress at the fracture site well over the fatigue limit.

The two primary factors that caused the fatigue failure were increased hardness and increased wear. The hardness change was evidenced by the microstructural analysis and the mechanical hardness tests. Hardness and brittleness are also closely linked. The implanted material was shown to be more brittle, which creates an environment for crack propagation rather than the stress distributing through ductile deformation. The increased density of dislocations, shown in the microstructure, increases both the hardness and likelihood of crack propagation.

The wear sites created opportunity for cracks to propagate, as scratches and pits introduced micro stress concentration sites. The wear resistance of the material both increased and decreased in different aspects. The material became more wear resistant as a result of hardening, which made the material more brittle and prone to cracking. The material also experienced pitting and scratching in the body, which created areas for more wear to occur. The physical wear resistance should not be confused with the corrosion resistance. The material experienced significant corrosive wear that introduced sites for crack propagation.

## 7.3.   Tibial Intramedullary Nail

Although included earlier in this paper, the images of the tibial intramedullary nail failure are shown in Figure 55.

Figure 55. The x-ray and regular image show the bend in the tibial
intramedullary nail.

The x-ray only shows floating fragments, and not the implant at the time of

failure. No outside evidence supports the reasons for failure, although the alterations in

mechanical properties are not assumed to have caused the fracture single-handedly.

### 7.3.1. Failure Analysis

The failure mode for the tibial intramedullary nail was the same as the short

femoral nail. High stress and many cycles contributed to a fatigue failure along with

several observed failure causes.

The mechanical properties in the tibial implant did not seem to change

significantly except for the failure site. The mechanism is still unknown but the section

that was changed was the section that failed. The failure site experienced increased

roughness, which indicates that corrosion and scratching has occurred. The similarity in situation to the short femoral implant leads us to assume similar failure causes.

## 7.4. Femoral Plate

The femoral plate appeared to have failed by brittle fracture. The fracture was sudden and a result of sudden loading rather than fatigue and crack propagation.

The hardness data showed that there was not a significant increase in the implanted sample. The roughness data in Chapter 6 an Figure 46  showed a significant increase, but the difference can be seen in macro-scratches on the surface. The damage on the surface was created during removal, and is not considered in the failure cause. The corrosion data shows no significant differences, and the small differences are attributed to the physical damage the implant sustained during removal. Considering the corrosion resistant properties of titanium, this assumption is reasonable. The body's effect on the mechanical properties of the titanium implant is considered negligible and the implant snapped from one of the causes listed in the introduction.

## CHAPTER VIII

## CONCLUSIONS

### 8.1. Conclusions

This thesis researched the effects of the human body on the material properties of metals used for internal fixation devices. The effects were studied on macro-mechanical, micro-mechanical, chemical, and morphological parameters. The results have identified a potential hazard to internal fixation and a common factor in the somewhat frequent event of fixation failure. The following conclusions have been established by this research.

- The simulation identified stress concentrations in the femur which doctors should be aware of to avoid aligning high stress areas on implant devices.

- The human body has significant effects on the mechanical, chemical, and morphological properties of stainless steels that have been used in bone fixation.

- The effect on the mechanical properties has ultimately led to a change in hardness and the roughness of stainless steel in the femur.

- The mechanical properties of titanium are not significantly altered while implanted in the human body. This criterion should be considered among many when deciding which implant material to use.

Typically the study of biomechanical implants in the human body focuses on the effects that the metals have on the human body. This research introduces an alternative approach in evaluating the implants. As the internal fixation industry grows to improve

human quality of life, reliability of the material will be crucial. The science of bone fixation is continually refining, and factors that affect failures are inevitably more controlled as time progresses.

## 8.2.  Future Recommendation

Future focus is suggested to obtain greater variety of samples. Samples of different materials and from different bones could expand the understanding of the effects of the body on material properties. Modeling of more human bones and even adding models of the metal implants would provide data to build an understanding of the effects of stress on change in material properties.

# REFERENCES

1.      Broos, P. and A. Sermon, *From unstable internal fixation to biological osteosynthesis. A historical overview of operative fracture treatment.* Acta chirurgica Belgica, 2004(4): p. 396-400.

2.      R. Rohilla, A.D., N.K. Magu, R. Singh, R. Siwach, *Fracture Dislocation of Elbow With Intra-Articular Displacement of Medial Epicondyle: A Report Of Two Cases.* The Internet Journal of Orthopedic Surgery, 2008. **8**(2): p. 5-10.

3.      McKibbin, B., *The biology of fracture healing in long bones.* The Journal of bone and joint surgery. British volume, 1978. **60-B**(2): p. 150-162.

4.      Aro, H.T. and E.Y.S. Chao, *Bone-Healing Patterns Affected by Loading, Fracture Fragment Stability, Fracture Type, and Fracture Site Compression.* Clinical Orthopaedics and Related Research, 1993. **293**: p. 8-17.

5.      Gotman, I., *Characteristics of metals used in implants.* Journal of endourology / Endourological Society, 1997. **11**(6): p. 383-389.

6.      Gurappa, I., *Characterization of different materials for corrosion resistance under simulated body fluid conditions.* Materials Characterization, 2002. **49**(1): p. 73-79.

7.      Bordjih, K., et al., *Evaluation of the effect of three surface treatments on the biocompatibility of 316L stainless steel using human differentiated cells.* Biomaterials, 1996. **17**(5): p. 491-500.

8.    Williams, D.F. and G. Meachim, *A combined metallurgical and histological study of tissue-prosthesis interactions in orthopedic patients.* Journal of Biomedical Materials Research, 1974. **8**(3): p. 1-9.

9.    Zimmerman, K.W. and H.J. Klasen, *Mechanical failure of intramedullary nails after fracture union.* J Bone Joint Surg Br, 1983. **65**(3): p. 274-5.

10.   Nabi, D.G., et al., *Radiologically visible surgical error and poor outcome of internal fixation in distal femoral fractures.* Ortop Traumatol Rehabil, 2008. **10**(4): p. 362-6.

11.   Collinge, C., B. Hartigan, and E.P. Lautenschlager, *Effects of surgical errors on small fragment screw fixation.* J Orthop Trauma, 2006. **20**(6): p. 410-3.

12.   Rho, J.Y., M.C. Hobatho, and R.B. Ashman, *Relations of mechanical properties to density and CT numbers in human bone.* Medical Engineering & Applied Physics, 1995. **17**(5): p. 347-355.

13.   Kanis, J.A., et al., *The diagnosis of osteoporosis.* Journal of Bone and Mineral Research, 1994. **9**(8): p. 1137-1141.

14.   Archer, D., *EDIS Update*, in *Families & Consumers : New and revised publications from the University of Florida Insitute of Food and Agricultural Sciences*: University of Florida, 2008.

15.   Kim, W.-Y., et al., *Failure of intertrochanteric fracture fixation with a dynamic hip screw in relation to pre-operative fracture stability and osteoporosis.* International Orthopaedics, 2001. **25**(6): p. 360-362.

16.     Swiontkowski, M.F., et al., *Torsion and bending analysis of internal fixation techniques for femoral neck fractures: The role of implant design and bone density.* Journal of Orthopaedic Research, 1987. **5**(3): p. 433-444.

17.     Newman Jr, J.C. and I.S. Raju, *An empirical stress-intensity factor equation for the surface crack.* Engineering Fracture Mechanics, 1981. **15**(1–2): p. 185-192.

18.     Centre, T.I. *Yield Strength*. 2006  [cited 2012 15 Sept 2012]; Available from: http://www.tppinfo.com/defect_analysis/yield_strength.html.

19.     Cahoon, J., W. Broughton, and A. Kutzak, *The determination of yield strength from hardness measurements.* Metallurgical and Materials Transactions B, 1971. **2**(7): p. 1979-1983.

20.     Pavlina, E.J. and C.J. Van Tyne, *Correlation of Yield Strength and Tensile Strength with Hardness for Steels.* Journal of Materials Engineering and Performance, 2008. **17**(6): p. 888-893.

21.     Hansen, N., *Hall–Petch relation and boundary strengthening.* Scripta Materialia, 2004. **51**(8): p. 801-806.

22.     Sasada, T., M. Oike, and N. Emori, *The effect of abrasive grain size on the transition between abrasive and adhesive wear.* Wear, 1984. **97**(3): p. 291-302.

23.     Khruschov, M.M., *Principles of abrasive wear.* Wear, 1974. **28**(1): p. 69-88.

24.     Bayer, R.G. and R.A. Schumacher, *On the significance of surface fatigue in sliding wear.* Wear, 1968. **12**(3): p. 173-183.

25.     Waterhouse, R.B., *Fretting wear.* Wear, 1984. **100**(1–3): p. 107-118.

26.    Reshetnyak, H. and J. Kuybarsepp, *Mechanical properties of hard metals and their erosive wear resistance.* Wear, 1994. **177**(2): p. 185-193.

27.    Suh, C.M., R. Yuuki, and H. Kitagawa, *Fatigue Microcracks in a Low Carbon Steel.* Fatigue & Fracture of Engineering Materials & Structures, 1985. **8**(2): p. 193-203.

28.    Ritchie, R.O., *Mechanisms of fatigue-crack propagation in ductile and brittle solids.* International Journal of Fracture, 1999. **100**(1): p. 55-83.

29.    Gaebler, C., et al., *Fatigue Strength of Locking Screws and Prototypes Used in Small-Diameter Tibial Nails: A Biomechanical Study.* The Journal of Trauma and Acute Care Surgery, 1999. **47**(2): p. 379-384.

30.    Eveleigh, R.J., *A review of biomechanical studies of intramedullary nails.* Medical Engineering &amp; Physics, 1995. **17**(5): p. 323-331.

31.    Haidukewych, G.J. and D.J. Berry, *Salvage of Failed Internal Fixation of Intertrochanteric Hip Fractures.* Clinical Orthopaedics and Related Research, 2003. **412**: p. 184-188.

32.    Schemitsch, E.H. and R.R. Richards, *The effect of malunion on functional outcome after plate fixation of fractures of both bones of the forearm in adults.* J Bone Joint Surg Am, 1992. **74**(7): p. 1068-78.

33.    MDGuidlines. *Malunion and Nonunion of Fracture*. 2012; Available from: http://www.mdguidelines.com/malunion-and-nonunion-of-fracture.

34.    Arens, S., et al., *Influence of Materials for Fixation Implants on Local Infection.* Journal of Bone & Joint Surgery, British Volume, 1996. **78-B**(4): p. 647-651.

35.    Dillin, L. and P. Slabaugh, *Delayed wound healing, infection, and nonunion following open reduction and internal fixation of tibial plafond fractures.* The Journal of Trauma, 1986. **26**(12): p. 1116-1119.

36.    Foundation, A. *Classifications of wound infection: chronic infection*. 2012; Available from: https://www2.aofoundation.org/.

37.    Voggenreiter, G., et al., *Immuno-inflammatory tissue reaction to stainless-steel and titanium plates used for internal fixation of long bones.* Biomaterials, 2003. **24**(2): p. 247-54.

38.    Ailinger, R.L., D.C. Harper, and H.A. Lasus, *Bone up on osteoporosis. Development of the Facts on Osteoporosis Quiz.* Orthop Nurs, 1998. **17**(5): p. 66-73.

39.    Hannan, M.T., et al., *Risk Factors for Longitudinal Bone Loss in Elderly Men and Women: The Framingham Osteoporosis Study.* Journal of Bone and Mineral Research, 2000. **15**(4): p. 710-720.

40.    Altair, E. *Linear Static Analysis*. 2012  [cited 2012 Oct 2]; Available from: http://training.altairuniversity.com/structural/linear-static-analysis/.

41.    Munting, E. and M. Verhelpen, *Mechanical simulator for the upper femur.* Acta Orthop Belg, 1993. **59**(2): p. 123-9.

42.    Tencer, A.F., et al., *Femur fractures in relatively low speed frontal crashes: the possible role of muscle forces.* Accid Anal Prev, 2002. **34**(1): p. 1-11.

43.    Grisso, J.A., et al., *Risk Factors for Falls as a Cause of Hip Fracture in Women.* New England Journal of Medicine, 1991. **324**(19): p. 1326-1331.

44.     Azom, M. *Stainless Steel - Grade 316L - Properties, Fabrication and Applications*. Azom.com The A to Z of Materials [Technical article] 2004 Feb 18, 2004 [cited 2012 09/02/2012]; Available from: http://www.azom.com/article.aspx?ArticleID=2382.

45.     Azom, M. *Titanium Alloys - Physical Properties*. 2002  [cited 2012 09/02/2012]; Available from: http://www.azom.com/article.aspx?ArticleID=1341.

46.     Vectran. *Tensile Properties*.  [cited 2012 09/02/2012]; Liquid Crystal Polymer Fiber]. Available from: http://www.vectranfiber.com/BrochureProductInformation/TensileProperties.aspx.

47.     Disegi, J.A. and L. Eschbach, *Stainless steel in bone surgery.* Injury, 2000. **31**: p. D2-D6.

48.     ASTM, *Specification For Wrought 18chromium-14nickel-2.5molybdenum Stainless Steel Bar And Wire For Surgical Implants (Uns S31673)*, 2008, ASTM International: West Conshohocken, PA.

49.     ASTM, *Specification For Titanium And Titanium Alloy Bars And Billets*, 2011, ASTM: American Society Testing and Materials: West Conshohocken, PA.

50.     ASTM, *Test Method For Knoop And Vickers Hardness Of Materials*, 2011, ASTM: American Society Testing and Materials: West Conshohocken, PA.

51.     Gadelmawla, E.S., et al., *Roughness parameters.* Journal of Materials Processing Technology, 2002. **123**(1): p. 133-145.

52.    Enos, D. and L. Scribner, *The Potentiodynamic Polarization Scan.* Technical
       Report 33, 1997. Scribner Associates Inc. University of Virginia.

53.    Mehl, R.F., *Metals Handbook.* Vol. 7: Atlas of Microstructures of Industrial
       Alloys. 1972, Materials Park, OH: American Society for Metals.

54.    gowelding.com. *Austenitic Stainless Steels*. 2004; Available from:
       http://www.gowelding.com/met/index.htm.

55.    Hornbogen, E., *The role of fracture toughness in the wear of metals.* Wear, 1975.
       **33**(2): p. 251-259.

56.    Bayer, R.G. and J.L. Sirico, *The influence of surface roughness on wear.* Wear,
       1975. **35**(2): p. 251-260.

57.    http://fibroblast.org. *Fibroblasts General Information*. Available from:
       http://fibroblast.org.